Numeric Benchmark Study of Plate Vibration Experiments in Air and Water

by
Karl R. Britsch

A Project

submitted to

Oregon State University

University Honors College

in partial fulfillment of
the requirements for the
degree of

Honors Baccalaureate of Science in Nuclear Engineering
(Honors Scholar)

Presented May 26, 2015
Commencement June 2015

AN ABSTRACT OF THE PROJECT OF

<u>Karl R. Britsch</u> for the degree of <u>Honors Baccalaureate of Science in</u>
<u>Nuclear Engineering</u> presented on <u>May 26, 2015</u>. Title:
<u>Numeric Benchmark Study of Plate Vibration Experiments in Air and Water</u>

Abstract approved: _____

Wade Marcum

A set of experimental plates were characterized to understand their dynamic response
in both air and water; in support of work performed at the Hydro-Mechanical Fuel
Test Facility and the Global threat Reduction Initiative. In an attempt to gain further
insight into the vibration of the experimental test plates, a numeric benchmark study
was performed to calculate their fundamental frequencies for vibration in both air and
water, employing a novel modeling method to simulate submersion; one which allowed
both the plate and the fluid domain to be modeled in the same numeric software
package. Results show that the air simulation compares well with the analytic
solutions; however comparison against experimental data is challenging, with no
obvious trends present. Given the available experimental data, select air simulations
are quite accurate, and careful selection of boundary conditions for other boundaries
yields representative results. For simulations of plates submerged underwater, larger
data sets for both experimental and numeric will be required to establish trends with
a high degree of confidence; however preliminary results suggest the method can be
accurate to a first order approximation, requiring minimal computational resources

Key Words: Plate Vibration, Finite Element Analysis, Submerged Vibration

Corresponding e-mail address: KarlRBritsch@gmail.com

Numeric Benchmark Study of Plate Vibration Experiments in Air and Water

by
Karl R. Britsch

A Project

submitted to

Oregon State University

University Honors College

in partial fulfillment of
the requirements for the
degree of

Honors Baccalaureate of Science in Nuclear Engineering
(Honors Scholar)

Presented May 26, 2015
Commencement June 2015

Honors Baccalaureate of Science in Nuclear Engineering project of Karl R. Britsch
presented on May 26, 2015.

APPROVED:

_____

Wade Marcum, Mentor, representing Nuclear Engineering

_____

Andrew Klein, Committee Member, representing Nuclear Engineering

_____

Brian Woods, Committee Member, representing Nuclear Engineering

_____

Toni Doolen, Dean, University Honors College

I understand that my project will become part of the permanent collection of Oregon
State University, University Honors College. My signature below authorizes release of
my project to any reader upon request.

_____

Karl R. Britsch, Author

ACKNOWLEDGEMENTS

TABLE OF CONTENTS

TABLE OF CONTENTS

Section   Page

LIST OF FIGURES

LIST OF FIGURES

1 –Introduction

In an attempt to gain further insight and understanding of submerged plate vibration, a suite of experiments were conducted at Oregon State University (OSU) to characterize the natural frequencies of a set of plates, vibrating in both air and water. Since experimental testing can be a tedious and time consuming endeavor, it is desirable to have different methods available for the purpose of calculating the natural frequency of any given plate, under the desired boundary conditions. Various analytic equations do exist; however they are often limited in scope and accuracy. Numeric analysis is becoming increasingly powerful; although, it too has a large share of uncertainty and can easily become error prone due to inconsistencies between a model and reality. In order to improve the accuracy of numeric methods, it is desirable to benchmark numeric results against both analytic and experimental data sets. For submerged vibration, numeric modeling is challenging due to the coupled nature of the plate and fluid domain; therefore the ability to solve submerged vibration problems numerically, in a simple and timely manner, is of even greater interest. The submerged plate modeling in this study employs the method outlined in the previous study Characterizing Virtual Mass Effects of a Submersed Body Using Pseudo-Fluid Elements [1], which was developed for submerged body vibration responses and has not been benchmarked against experimental submerged plate vibration.

1.1   Motivation

It is the intent of the National Nuclear Security Agency, through their Global Threat Reduction Initiative, to convert all civilian research and test reactors from highly enriched Uranium fuel to low enriched Uranium fuel. In recent cases, such conversions require the qualification of a new fuel material. In 2012, an irradiation test in the Advanced Test Reactor (ATR) located at the Idaho National Laboratory (INL)

resulted in a plate, at the end of the test assembly, sheering off in-pile. This was later hypothesized to be the result of vortex shedding off an upstream element near the fundamental frequency of the plate.[2] Due to the unexpected nature of this failure, a series of experiments were conducted at OSU with the goal of characterizing the natural frequencies of a set of small test plates that are geometrically similar to the prototypical low enriched Uranium fuel plates, to ensure that such a failure will not occur. These experiments, called the *Vibration in Thin Fluid Channel Bench-Top Experiment (VFC)*, [3] are the basis of all work performed during this study.

The VFC experiments involve a set of small plates, approximately 1 inch wide, with lengths varying between 0.35 inches and 4 inches. Fourteen of the plates are comprised of either homogeneous Aluminum or Inconel, with an additional laminate plate; consisting of a thin Depleted Uranium (DU) – Molybdenum foil, encased within Aluminum cladding, which will be referred to herein as the DU Plate. Each plate was held in a clamping device and vibration data was collected by a strain gage while the plate was plucked with a guitar pick. The temporal strain gage data was transformed into the frequency domain through use of a Fast Fourier Transform, and the natural frequency was identified through observation of the first prominent peak of the range of frequencies. [3]

The plate holders, shown in Figure 1.1, were designed to represent idealized boundary conditions and employed three different designs, all of which clamped the plates along their 'length' (l), leaving the 1 inch 'width' (w) of the plate free to vibrate on both ends. The first two holders clamped down securely on the plate, and are thus referred to as 'clamped plate' holders; one of which compressed the plate between two flat surfaces, as shown in Figure 1.2, the other of which compressed the plate at a single point down the length of the plate, providing a pined line, shown in Figure 1.3. These two are respectively referred to as the 'flat-edge' and the 'knife-edge' clamping devices. The last holder, called the 'sinusoidal slot,' employed two grooves cut into the sides, which the plate slid into. Each of these grooves follows a very slight sinusoidal wave, with the intent of simulating point contacts where the groves impinged upon the plate, shown in Figure 1.4.
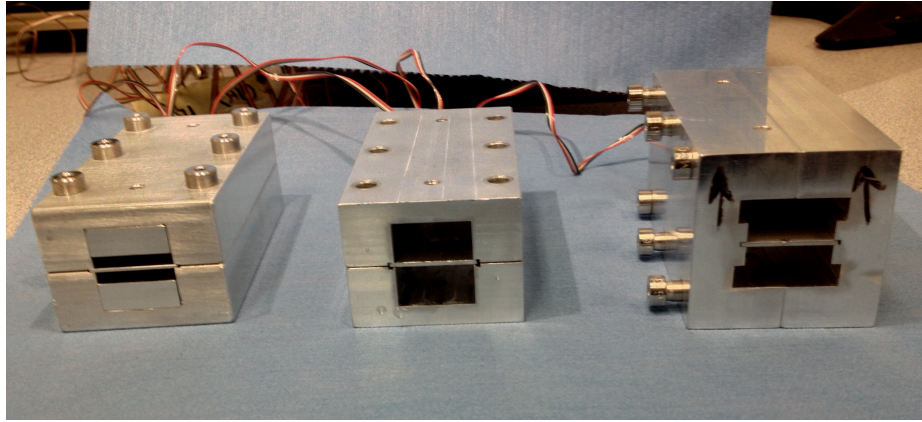
Figure 1.1: **VFC Plate Holders** - Flat edge holder with gap inserts, knife edge holder, and the sinusoidal clamping device with arrows indicating the In-Phase configuration
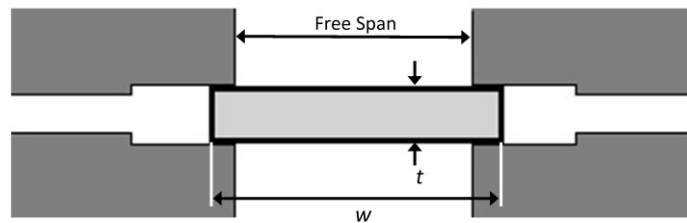
Figure 1.2: **Flat Edge Clamping Device** - Section through the width of the flat edge clamping device with plate.
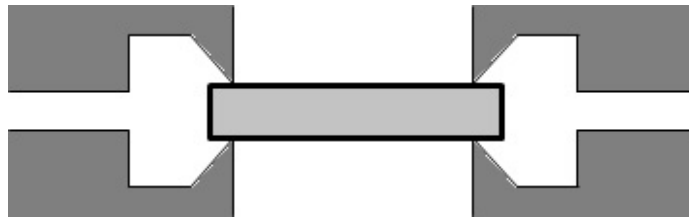
Figure 1.3: **Knife Edge Clamping Device** - Section through the width of the knife edge clamping device with plate.
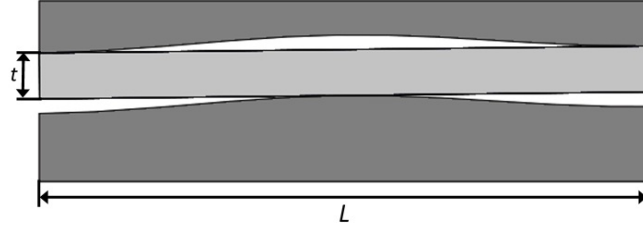
Figure 1.4: **Sinusoidal Slot Clamping device** - Section showing the Sinusoidal Slot and a non-deformed plate.

1.2   Objectives

It is the objective of this study to examine the accuracy with which a set of numeric techniques may be employed to calculate the fundamental frequency of a plate vibrating in air and water, under a variety of boundary conditions and plate materials. The bulk of the results will focus on comparisons with the set of vacuum simulation results and between the results and experimental data, in order to establish trends. Submerged work will focus on the ability of the numeric solver to simulate the pseudo-fluid elements and the interaction these elements create with the plate. Comparisons between submerged numeric results and experimental data will be made; however it is beyond the scope of this work to perform a rigorous error analysis upon the pseudo-fluid simulations. Ultimately the comparisons presented will yield a qualitative level of confidence in the ability to predict the natural frequency of plates via numeric means.

1.3   Document Overview

This document opens with a literature review, before discussing the set-up of the simulated models and going into the details of simulation work. The methods section provides the details behind the analytic and numeric work, first deriving the analytic equations used in model verification, then emphasizing the analytic methods used

to check the numeric solution accuracy, before detailing numeric modeling methods and assumptions. The results section contains an overview of the results, comparing them against each other and experimental data in order to discuss the validity of the methods. The paper closes with concluding remarks and suggestions for further work. All tabulated values from numeric, analytic, and experimental data are listed in Appendix A and detailed error analysis calculations, including supporting calculations and intermediate calculated values, are shown in Appendix B.

2 –Survey of Literature

Vibration is a common topic for research within the field of engineering that has a long history and a well developed theory for many common circumstances. However, the transition from theory to application, through equations or correlations, is an ongoing study. Plate vibration in particular, is a common subdivision for research, due to the plethora of plates found in everyday structures, as well as the many commonalities between plates and two dimensional beams. A plate is defined as any structure in which one of the dimensions is substantially shorter than the other two dimensions; [4] helpfully allowing analytic plate theory to be derived with the same approach used to derive beam theory. Beam theory is widely understood, and represents some of the original vibration theory for solid bodies; it was first derived by Bernoulli, and then improved upon by Euler, creating what is commonly called Euler-Bernoulli Beam Theory. This theory is widely applicable and, due to its simplicity and relative accuracy, is still in widespread use. [5] Considering a plate to be a beam with an extra dimension, the same methods outlined in beam theory may be applied, yielding differential equations that describe plate vibration. [6] As with any analytic work, certain assumptions are required to derive the Euler-Bernoulli Beam equations, and the corresponding limitations of these assumptions limit the applicability of beam theory; chiefly, the assumption of a slender beam, or correspondingly, a thin plate. Other approaches have been derived to allow analysis of thick plates, such as an expansion upon The Timoshenko Beam Theory, which assumes a non-slender beam, ultimately yielding Midlin-Timoshenko Plate Theory. [6] In either approach, once the assumptions have been identified, the equations of motion are combined with an analytic description of the boundary conditions to arrive at a set of differential equations. Once solved, these equations will yield the hypothetically exact analytic solutions for certain plate frequencies, at which the corresponding wavelengths are integer multiples of the plate's length, allowing the development of standing waves.

However, in the best of cases, solving these differential equations is complicated, and for some boundary conditions, impossible. Silva, in <u>Vibration Fundamentals</u> shows one such solution, ultimately requiring an educated guess and yielding an infinite sum. [7]

Due to the complexities of purely analytic solutions, other means have been developed to an analytic approach, without the complex mathematics, often through the use of tabulated Eigen values. One such set of equations and tabulated values is provided by Blevins in <u>Formulas for Natural Frequency and Mode Shape</u> [8], which lists Eigen values for a wide range of boundary conditions, plate modes, and plate geometries. The tabulated Eigen values are multiplied into a base equation, describing the plate's material properties. Belivin's employs the equation for flexural rigidity, with density divided out, as the base equation for plates vibrating in air. While this method is far easier to use, it is limited by the extent of the reference, and has no error estimate applied to it which could lead to questionable accuracy. Furthermore, since the multiplication factors are listed only at explicit plate geometries, care must be taken when extrapolating or interpolating to the geometry of interest.

Finite element analysis is another method commonly utilized in vibration analysis, and is becoming increasingly powerful. Kerboua et al. [9] and Hamedani et al. [10], both derive and write their own computational codes to numerically solve for the fundamental frequencies of flat plates vibrating in air. Hamedani compares the accuracy of traditional rectangular elements against 'super elements' for stiffened flat rectangular plates, finding that the traditional elements had better accuracy and convergence characteristics than the 'super elements,' though the solution was slower. [10] Kerboua derived a finite element code for non-uniform isotropic and anisotropic plates, finding good agreement with experimental results. [9]

The relative complexity of plate vibration is further increased by submergence of the plate in a fluid medium. Since air has a low density, its effect on vibration is minor and normally ignored. Solving for plates submerged in a damping fluid does not allow this luxury. The inertial and viscous properties of water provide resistance to movement of the plate, substantially changing the natural frequency of vibration

for any submerged object. Typically this resistance is analytically treated as added mass, where the mass of the water can be added to the plates mass and the frequency analytically solved using the new mass in the same manner as an isolated plate. This approach was first taken by Horace Lamb [11], in which the added mass effects of water on a circular plate were analytically derived and used to calculate the frequencies of submerged circular plates. A similar approach is taken by Haddara and Cao [12] who find good correlations between their analytic results and the experimental studies of Fu and Price. Further consensus is seen with another paper by Vu et al. [13] For both of these papers and their cited experimental work, it is seen that any submergence of a plate results in a decrease in frequency for all modes, with the damped frequencies asymptotically approaching some lower value as the depth of submergence increases; reaching an approximately constant value once the plate is submerged to about 50% of its length, with the exact depth varying slightly for differing plate edge ratios and different modes. Vu et al. further note that the first mode is the most effected by submergence, with higher modes seeing a decreasing effect from the added mass dampening.[13]

A paper by Pal et al. [14] also examines added mass effect on a laminate plate using an in-house finite element analysis software to model both the plate and the fluid domain. Their results are in good agreement with experimental data, and their ability to model laminated plates is a major advantage over previous mathematical treatments. However, their report did not include any information about submerged modeling, which they eventually intend to perform. Taking numeric modeling of submerged plate vibration a step further, Howard et al. model the plate and fluid domain in the commercial, off-the-self, finite element analysis software system, ABAQUS. In order to reduce the uncertainties associated with numerical computation of fluid-structure interactions, which are often solved by coupling a computational structural mechanics (CSM) solver to a computational fluid dynamics (CFD) solver, the water domain was modeled as a solid "pseudo-fluid" which was broken into discrete solid elements to be solved purely in the CSM domain. [1] Their findings are also in good agreement with experimental results; however, difficulties were encountered when modeling a fluid in

the solid domain and suggest that further experimental work is necessary to establish the limitations and uncertainties of the method.

In this study, the method outlined by Howard et al. will be used for modeling submerged plate vibration. Initially the ABAQUS frequency solver will be used to numerically find the fundamental frequencies of the plates. The associated accuracy of this method may be determined from comparison against experimental data, and the most accurate models will be coupled with pseudo-fluid elements for submerged plate modeling. This should allow for an acceptable comparison between numeric and experimental data, lending insight to the technique's accuracy. Further comparisons will be drawn from analytic equations provided by Blevins in <u>Formulas for Natural Frequency and Mode Shape</u>, for air vibration, in order to provide an additional resource for comparison in the case of discrepancies.

3 –System Design

The Vibration in Fluid Film Bench-top Experiment employs 15 small plates, which have the dimensions and material properties given in Table 3.1. Plates 1-9 and 15 (the DU Plate) employ a length to width ratio of 4:1, while plates 10-14 have varying aspect ratios that were chosen to fall within the set of ratios given in Formulas for Natural Frequency and Mode Shape [8], in order to provide analytic solutions for comparison against numeric results. The first 7 plates are homogeneous Aluminum, with varying thicknesses, and plates 8-14 are homogeneous Inconel of varying lengths.

The plates were modeled in ABAQUS/CAE, version 6.13-2, by Dassault Systèms-Simula Corp. as discrete, deformable, homogeneous bodies with the material properties shown in Table 3.1. To ensure continuity across all simulations, copies of the original set of plate models simulated for vacuum vibration, were used in subsequent submerged simulations, with different boundary conditions applied as needed.

3.1 Clamped Plate Models

The modeled boundary conditions attempt to mimic the conditions applied to the plates by the plate holders. Both of the clamped plate holders, shown in Figure 3.1, applied boundary conditions that could be simulated in similar fashions. They both have identical free span widths of 0.88 inches and clamp along the entire plate length. The free span of each plate was instrumented with a strain gage across the plate's width, and the plate was plucked by the experimenter on one of the short edges; thus it was assumed the free span was the only area of the plate vibrating, allowing the clamped plates to be modeled as having a width equivalent to the free span. The clamped boundary conditions were applied down the plate's length, at the reduced plate width, and were assumed to be ideal, such that the knife edge holder would only allow the plate to rotate at the boundary condition, limiting any translation, while the

flat edge holder was assumed to restrict both rotation and translation. In reality, the knife edge holder clamps down on both faces of the plate, greatly hindering rotation, so it is reasonable to assume that although the plate extends beyond the boundary, this small extension is unlikely to impact the natural frequency of the plate. This demonstrates the complexity of modeling boundary conditions; which, in order to gain as much insight as possible, were modeled for the clamped plate holders using three different sets of ideal boundary conditions:

- Fixed–Fixed (F-F)

- Fixed–Pinned (F-P)

- Pinned–Pinned (P-P)
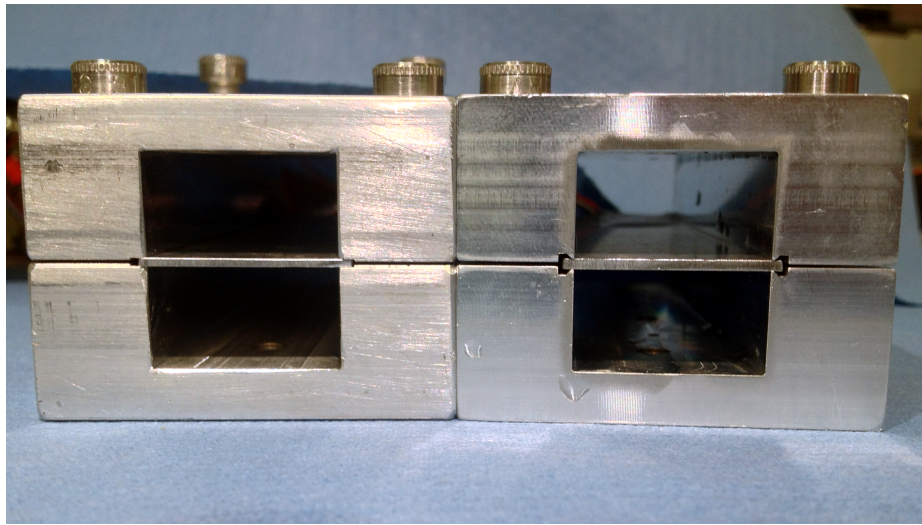
Figure 3.1: **Flat and Knife Edge Plate Holders** - The two clamping fixtures with plates installed showing the difference in boundary conditions

In ABAQUS, ideal conditions are set up such that a Pinned boundary condition, restricts all translation, but puts no limit on rotation. A Fixed condition, called "Encastered" in ABAQUS, completely restricts both translation and rotation. One caveat does arise when using these ideal conditions, the Pinned boundary must be

applied to a line; otherwise the conflicting translation restrictions prevent rotation, effectively creating a fixed condition. Unfortunately, line contacts result in high local stress concentrations, which decreases the accuracy of the computation. To help alleviate some of the issues, the Pinned condition was applied down the middle of the boundary face and the decreased accuracy was taken into consideration by performing all error analysis calculations on the P-P boundary condition.

Table 3.1: Plate Dimensions and Materials

Plate	Length (mm)	Width (mm)	Thickness (mm)	Young's Modulus (Pa)	Poison's Ratio	Density (kg/m^3)
1	102.2	25.40	1.524	6.89 E+10	0.33	2700
2	101.4	25.40	1.524	6.89 E+10	0.33	2700
3	101.6	25.40	1.194	6.89 E+10	0.33	2700
4	101.6	25.40	0.940	6.89 E+10	0.33	2700
5	101.6	25.50	1.524	6.89 E+10	0.33	2700
6	101.6	25.58	1.194	6.89 E+10	0.33	2700
7	101.6	25.48	1.194	6.89 E+10	0.33	2700
8	101.5	25.40	1.245	2.05 E+11	0.32	8200
9	101.5	25.40	1.245	2.05 E+11	0.32	8200
10	56.31	25.32	1.245	2.05 E+11	0.32	8200
11	33.38	25.32	1.245	2.05 E+11	0.32	8200
12	22.61	25.32	1.245	2.05 E+11	0.32	8200
13	14.99	25.32	1.245	2.05 E+11	0.32	8200
14	8.890	25.32	1.245	2.05 E+11	0.32	8200
15 Cladding	101.6	25.32	1.245	6.89 E+10	0.33	2700
15 DU Foil	82.55	19.05	0.330	8.73 E+10	0.324	17130

3.2   Sinusoidal Slot Models

The Sinusoidal Slot boundary conditions were created by a groove cut into the side of the plate holder block, which the plate slides into. The groove shape is effectively a sine wave, which undergoes a complete period over the plate length; giving a free vibration span of 0.88 inches. The two opposing sides of the plate holder may be taken apart, so that the grooves may be flipped relative to one another, allowing both grooves to bend the same direction, labeled 'In–Phase,' or bend opposite of one another, labeled 'Out–of–Phase,' as shown in Figures 3.2 and 3.3. The sinusoidal shape of the groove deforms the plate slightly, and the resulting contact between the holder and the plate is not continuous – as seen in the clamped cases. Instead, the contacts can be modeled as line contacts across the depth of the groove at the locations where the holder and plate meet, shown in Figure 3.4.

Figure 3.2: **In Phase Sinusoidal Holder** - In Phase slot paths shown for both sides of the holder
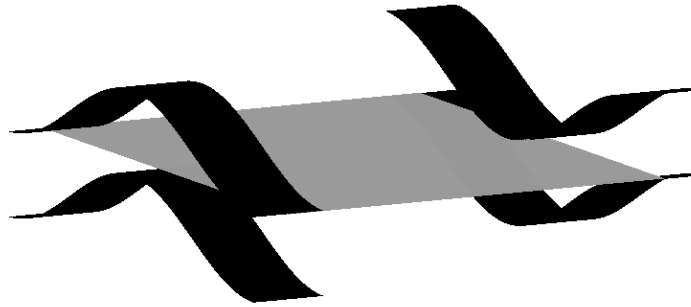
Figure 3.3: **Out of Phase Sinusoidal Holder** - Out of Phase slot paths shown for both sides of the holder
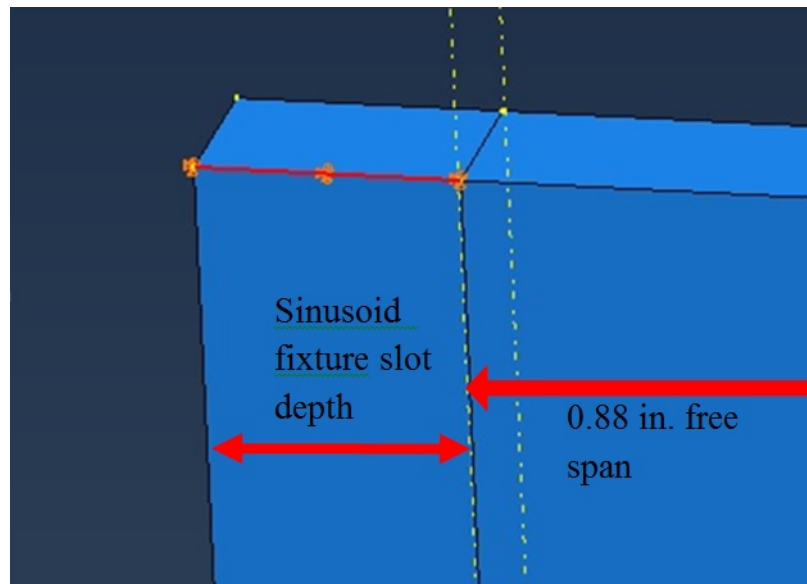
Figure 3.4: **Flat Plate in Sinusoidal Clamping** - Plate with the slot depth sectioned out, showing line contact

Ultimately, the complex interactions between the plate and the Sinusoidal Slot holder require further analysis than the simple line contacts from Figure 3.4. The plate is held securely enough that translation is unlikely; however it may still chatter because the slot is cut taller than the thickness of the plate. Additionally, the exact shape of the plate within the holder is unknown, and dependent upon numerous conditions, including plate thickness. The the Sinusoidal Slot holder was manufactured to mimic ideal line contacts on an undeformed plate, where the line would be infinitely thin, touching across the depth of the grove. However, to address the observed behavior of the holder, two simulation methods were attempted; the first modeled the ideal design of the slot, considering the plate to be lying flat, with line contacts at the exact location where the groove impinged upon the plate, as given by a sine wave undergoing a complete period over the plates length; shown in Figure 1.4. To further refine results, the second set of simulations considered a deformed plate; first taking the original plate and bending it into a shape similar to the sinusoidal slot. A series of translating boundary conditions at the contact locations were used to deform the plate 'up' or 'down' relative to the plate's thickness (along the Z-axis), before solving for the frequency. However, the translating boundary conditions cause far too much stress for line contacts to be used, instead relying on a more physically representative 'area contact' to account for the expectation that the slot contacts the plate over a small area. Additionally, it was established that larger area contacts caused the solutions to converge upon the clamped plate results; so a contact length of 1/8 inch were chosen, applied as shown in Figure 3.5. The area contacts did not result in unrealistic stress concentrations, but did cause the plate to translate along its length slight while bending into the sinusoidal shape; eliminating the use of ABAQUS's pre-programmed Encastered or Pinned conditions. Instead limitation boundary conditions were used, restricting motion along the plate's Z-axis after the boundary translation was complete. The exact Z displacement did not have a major impact on the frequency, so long as the distance was small relative to the plate thickness. X and Y (width and length) limitations were also employed at the respective plate center-lines, to eliminate rigid body vibration of the plate. Applying the limitations at the plate centerline was found

to be preferable to the more simple application of an Encastered condition on a single corner, since the plate is allowed to deform towards the center of mass.
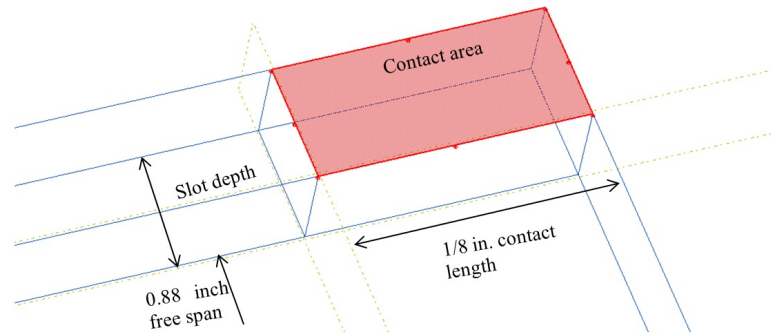
Figure 3.5: **Contact location detail** - Detail showing the contact area across which the boundary condition is applied for the deformed plate sinusoidal simulations.

3.3 Submerged Plates

Modeling submerged vibration of a plate is challenging, due to the added resistance of the fluid medium. While air does in fact add resistance, its effect is normally neglected due to the air's low density and viscosity; a luxury not permissible for submersion in water. Instead, the method outlined by Howard et al. [1] was applied, where the water domain was numerically modeled as a solid body.

This solid 'water' is created by examining the properties required to define a material in ABAQUS, which at minimum, consist of: density, Poison's Ratio, and Young's Modulus. Defining: mass, deformation characteristics, and stiffness. Density is a property of fluids, and may be directly applied to the 'water' material. Poison's Ratio is likewise simple, since it measures the resulting deformation along an axis, resulting from deformation along an orthogonal axis. Water will displace an equal volume, since it is roughly incompressible; giving a Poison's Ratio of 0.5. Young's Modulus of Elasticity must be treated differently; Howard et al. first examined the major difference between fluids and solids, noting that fluids do not propagate sheer

waves, having a sheer modulus of zero. The Elastic modulus may be calculated from the sheer modulus and Poisson's Ratio, leading to a Young's Modulus of zero. However, fluids do posses a property called the bulk modulus, which measures the compressibility of a fluid in response to a change in pressure. It was found to be necessary to calculate an effective Young's Modulus from the fluids bulk modulus, in order for the expected vibration damping to occur. The values used for the 'water' properties, are listed in Table 3.2, in which Poison's Ratio has to be modified to $\nu = 0.4999999$, to avoid a divide by zero error.

The 'water' models were created in the same fashion as the plate; discrete, deformable, homogeneous bodies, coupled to the X-Y surfaces of the plate using ABAQUS 'Tie' conditions, shown in Figure 3.6. Two separate 'water' bodies had to be modeled, since the submerged experiment used different channel gap inserts to narrow the gap between the faces of the plate and the inner surfaces of the holder. The experimenter designated the gaps either **A** or **B**, with the **A** gap being slightly thinner than the **B** gap. The size of the gap for clamped and sinusoidal holders differs slightly, with the measured values listed in Table 3.3. The 'water' was confined by boundary conditions designed to mimic the interior walls of the holder. The 'top' and 'bottom' faces of the water was subject to a Z axis limitation, while the 'left' and 'right' sides, were subject to X axis limitations; the pseudo-fluid bodies were still free to deform along the plate's length, the Y axis, since the holder is open on both 'ends' of the plate.

Table 3.2: Material Properties of Solid 'Water'

Property	Simulated Value	Units
ρ	1000	$[kg/m^3]$
E	13 200	[Pa]
ν	0.4999999	
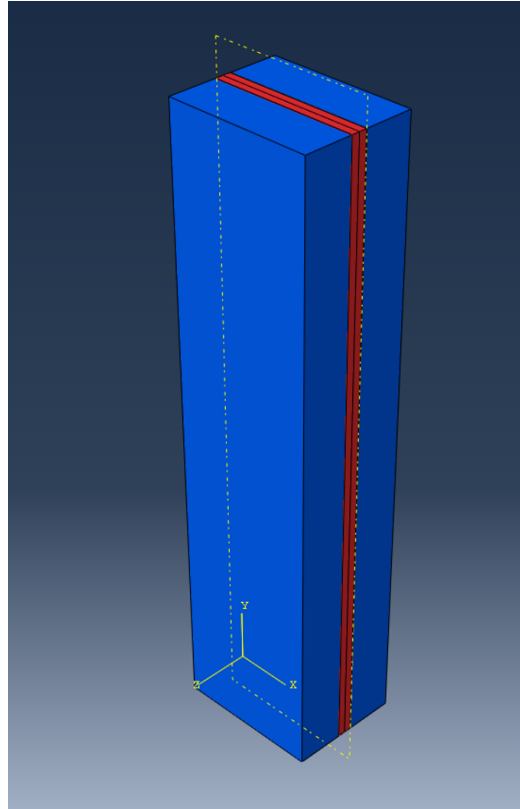
Figure 3.6: **Model of Plate and Water** - Model showing the plate, in red, coupled to the 'water,' in blue.

Table 3.3: Channel Gap Sizes

Designation	Clamped (mm)	Sinusoidal (mm)
A	2.90	1.70
B	3.78	2.60

3.4 General Considerations

Once the methods for simulating the plates were established, a final set of models were created with the given material properties from Table 3.1, copies of which were then modified for the applicable boundary conditions. Simulations with symmetric boundary conditions, P-P, F-F, and In–Phase, were modeled at half width, using an X-axis symmetry condition in place of the F, SS, or In-Phase contacts, dramatically reducing computation time, but limiting results to symmetric modes. The Sinusoidal Slot simulations had an additional limiting factor because only the plates that were 4 inches long and thin enough to fit in the slot could be tested, limiting these simulations to plates 3, 4, 6-9 and the DU plate.

The plates were meshed in ABAQUS using the default cubic mesh; a C3D8R hex mesh with first order linear extrapolation. The default conditions primarily were chosen for simplicity and in part to avoid additional separate effects studies, for the purpose of examining the effects of varying the mesh parameters. The laminate structure of the DU plate model prevented the use of a Hex mesh on the Aluminum cladding, which was instead meshed using the default C3D4R tetrahedral mesh, with first order accuracy and linear extrapolation. The DU foil was meshed with the default Hex mesh to maintain continuity. The pseudo-fluid models were modeled in an identical manner to the plates, with a C3D8R linear hex mesh to maintain continuity with the plate modeling and to ensure the model was solvable with the available computational resources. More advanced meshes were considered, such as a quadratic extrapolation elements, C3D20R, and hybrid elements, which allow ABAQUS to directly solve for the pressure loading on each element, C3D8RH or C3D20RH. Unfortunately the increased computational requirements of these mesh

elements greatly increased the solution time, making an extensive study of this analysis method impractical.

4 –Methods

Verification of the numeric models involved comparison against analytic solutions for air vibration. Clamped plate air vibration frequencies were readily calculated, using available equations from literature; however no analytic solution could be found for the sinusoidal holders. To address this, the numeric results for the clamped plates were compared for accuracy before any of the Sinusoidal Slot simulations were run, using the same set of plates.

4.1   Analytic Solutions

As accompaniment to the vacuum simulations, analytic work was performed to provide a set of verification solutions. Equation 4.1, presented by Blevins in Formulas for Natural Frequency and Mode Shape [8], was chosen to calculate the analytic solutions for the fundamental mode of a clamped plate vibrating in air, with either a P-P, F-P, or F-F boundary condition.

$$f_{ij} = \frac{\lambda^2}{2\pi a^2} \left[\frac{Et^3}{12\gamma(1 - \nu)} \right]^{\frac{1}{2}} \tag{4.1}$$

In this equation γ is the area density, equal to the plate density, ρ, multiplied by the plate thickness, t. E is the modulus of elasticity, a is the 'free span width' of the plate, and ν is Poisson's Ratio. The λ^2 value is a unitless number given in Natural Frequency and Mode Shape corresponding to: plate dimensions, clamping method, and plate vibration mode; where the plate mode is a combination of the number of half-waves along the plate's length, denoted by i, and width, denoted by j. The given λ^2 values from Natural Frequency and Mode Shape corresponding to the range of plate dimensions and VFC boundary conditions of interest, are shown in Table A.1. These values do not match up exactly with the geometries of the VFC plates, necessitating

extrapolation and interpolation to the desired edge length ratios; accomplished using quadratic best lines of the closest three consecutive given data points in Microsoft Excel. The resulting λ^2 values are shown in Table A.2.

The laminate nature of the DU plate necessitated further mathematical manipulation before it could be analyzed with Equation 4.1. In Predicting Critical Flow Velocity and Laminate Plate Collapse Flat Plates [15] the authors Jensen et al. analyze methods for analytically predicting critical flow velocity of a plate, with particular interest in laminated fuel plates. In order to surpass the multi-region nature of a laminate plate, the flexural rigidity term, D, is employed, where:

$$D = \frac{t^3}{12} \frac{E}{(1 - \nu^2)} \tag{4.2}$$

D may be used in calculation of the fundamental frequency of the plate by entering it into Equation 4.1 to give:

$$f_{ij} = \frac{\lambda^2}{2\pi a^2} \frac{D}{\overline{\gamma}}^{\frac{1}{2}} \tag{4.3}$$

In which $\overline{\gamma}$ signifies the average area density.

For laminated plates, Jensen et al. details two methods of deriving the flexural rigidity term, ultimately deciding the ideal laminate model, given in Equation 4.4, is the best suited over a wide range circumstances.

$$D = \frac{1}{3} \left(\frac{2E_{or}}{(1 - \nu_{or}^2)} \left(\frac{3}{4}(t_{ir}^2)t_{or} + \frac{3}{2}t_{ir} * t_{or}^2 + t_{or}^3 \right) + \frac{E_{ir}}{(1 - \nu_{ir}^2)} \frac{t_{ir}^3}{4} \right) \tag{4.4}$$

Equation 4.4 employs the subscripts ir and or to signify the inner and outer regions; additionally requiring that the two outer regions be identical to each other. The remaining unknown,$\overline{\gamma}$, in Equation 4.3 is an easily computed average:

$$\overline{\gamma} = \frac{\rho_{ir} * l_{ir} * t_{ir} * \rho_{or} * l_{or} * 2t_{or}}{l_{or} * w_{or}} \tag{4.5}$$

Using Equations 4.4 and 4.5 it is possible to solve for D, which may be used in Equation 4.3 to arrive at the fundamental frequency of the DU Plate vibrating in air.

4.2   Analytic Error Analysis of Numeric Results

The accuracy of numeric results depends upon the number of mesh elements used to calculate the solution. As the number of mesh elements goes to infinity, the model comes closer and closer to reality, and likewise becomes capable of modeling perturbations with higher precision; causing the calculated results to asymptotically approach a 'true' value. Grid dependence studies establish what this 'true value' is, allowing the error to be defined as the percent difference between the calculated result and the 'true value.' In order to ensure the simulation results accurately model reality, a grid dependence study was performed upon plates 1, 4, 10-14, and the DU plate for the most error prone boundary condition, the P-P condition. The same error analysis was also applied to plates 4, 7, and the DU plate for Sinusoidal Slot Plates with both the line and area contact assumptions. No submerged plate error analyses was carried out due to computational limitations. All detailed calculations of the error analysis may be found in Appendix B.

The derivation of the grid dependence study begins with considering the element size; as the number of elements goes to infinity, the size of each computational element trends to zero, a fact that can be leveraged by defining an element size, h, as the inverse of the number of elements along an arbitrary plate direction. Since the plates are thin compared to their length and width, it is convenient to define h as the inverse of the number of elements across the plate thickness:

$$h = \frac{1}{n_{i,z}} \tag{4.6}$$

Since the denominator trends to zero as we approach infinity, the change in element size, Δh, is preferred, where:

$$\Delta h_i = \left| \frac{1}{n_{i,z}} - \frac{1}{n_{i-1,z}} \right| \tag{4.7}$$

And correspondingly, the magnitude of the change in frequency, Δf, is compared against the change in elements size, where:

$$\Delta f_i = |f_i - f_{i-1}| \tag{4.8}$$

By keeping the element side length ratio constant, while simulating several different element sizes, it is possible to examine the change in element size against the change in frequency. These frequency changes are exponential in nature, so both equations are linearized through taking the natural log of Δf and Δh. The plot of linearized data, $\ln \Delta f$ as a function of $\ln \Delta h$, can have a linear trend line fit to it, which has well-known equation that describes the line for all Δh. This equation can be rewritten with respect to the variables of interest as:

$$\ln \Delta f = m * \ln \Delta h + b \tag{4.9}$$

in which, m and b are the slope and y intercept of the best fit line. It is now possible to describe the behavior of the data at any mesh element size, so long as the change in element size required to get from a known result, to another result, is known. Taking the last known result and using that element size as the next Δh value effectively changes the element size to zero. Rearrange Equation 4.9 for frequency allows the true frequency, f_{i+1} to be found:

$$f_{i+1} = f_i + e^{(m\Delta h_i + b)} \tag{4.10}$$

The percent error, also known as the percentage of exact value, was established from the difference between the true frequency and the last frequency result, divided by true frequency, and multiplied by 100%. When calculating the grid dependence, it is considered necessary to examine a minimum of 5 elements in any directions for the results to be meaningful, and the elements should be as close to cubic as possible. The dramatic difference between the length and width of the plates compared to the thickness, necessitated element edge length ratios of 2:2:1, with the elements being half as thick were long or wide.The mathematics work best if h is halved each step; implying that the number of elements along any direction must double each time. This

requirement suggests the grid dependency studies use steps of 5, 10 and 20 elements across a plate's thickness.

To avoid performing grid dependency studies on all 15 plates, the element size, h, was fixed at the size producing to 20 elements across the thickness of Plate 1, which has the largest volume. Using this element size, listed in Table A.3, it is possible to bound the expected error for Plates 1-9. Since the element size is set for Plate 1, this plate is expected to have the smallest error; while in contrast, the thinnest plate, number 4, should have the largest error because it will have the fewest elements. By performing a grid dependence study on Plate 4, with 5, 10, and 20 elements across the thickness, and comparing the 'true frequency' result to the simulation results at the fixed element size given in Table A.3, the largest expected error may be established as the percent difference of these two results. Error for the remaining seven plates will fall between that established for Plates 1 and 4.

Plates 10-14 have different edge length ratios, but identical thicknesses. Individual error analyses were carried out on each to eliminate any effects of edge length ratio on solution accuracy using the mesh element sizes are shown in Table A.3. The DU Plate also has its own error analysis to ensure no unexpected results cropped up from the tetrahedral mesh or the laminate model.

4.3   Submerged Plate Simulations

Upon the conclusion of air simulations, work on submerged plate vibration began. The first issue encountered was the failure of the Eigen solver. The low sheer modulus of the 'water' elements, result in fundamental frequencies far below the range of the plate, making it impossible for the Eigen solver to find a frequency for the plate. To surpass this difficulty, the plates were numerically 'plucked' by an applied pressure load that was instantaneously released so the displacement of the plate as a function of time could be tracked. By subjecting this displacement vs. time data to a Fast Fourier Transform (FFT), frequency data was obtained, from which the first prominent peak was taken as the fundamental frequency. To ensure this method would work, it was

first attempted upon an isolated plate, mimicking air vibration, and the frequency results were compared against the Eigen solver results. It was found that most loading schemes excited high order modes, which slightly modified the fundamental frequency found in the Fourier Transform. Figures 4.1 and 4.2 show two pressure loads used to 'pluck' the isolated plate. Figure 4.1 mimics the experimental loading, of pressing one free end of the plate with a guitar pick, while in Figure 4.1 attempts to deform the plate into the fundamental mode shape for vacuum vibration. As shown in Figure 5.13, it was found that Figure 4.2 gave superior results for air vibration; however, coupling the pseudo-fluid elements to the plate interfered with the mode shape. As a result, the pressure loading shown in Figure 4.3 was finally selected for 'plucking' the submerged plates.

The water was coupled to the plate through tie interfaces, and the assembly was meshed for numeric solutions. Numerically, solving for plate vibration as a dynamic step is far more computationally expensive than the Eigen solver was. In order to arrive at solutions in reasonable periods of time, both the plate and water meshing was kept as coarse as possible. The plate was meshed at 10 elements across the plates thickness, using the same 2:2:1 element edge length ratio as for the Eigen simulations. The 'water' was meshed using cubic cells, aiming at 8-10 across the thickness of each water model, which gave element sizes quite a bit larger, listed in Table A.3.
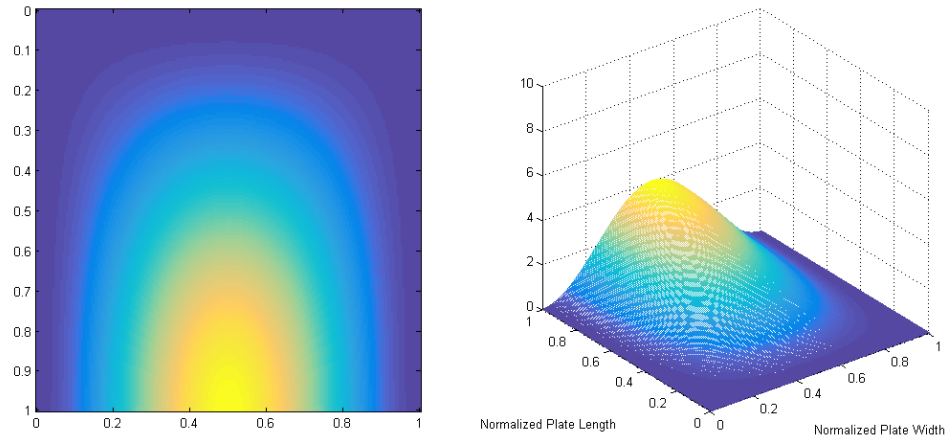
Figure 4.1: **Guitar Pick Pressure Loading** - Pressure loading attempting to simulate experimental plate pluck using guitar pick on one open end of the plate. The plate dimensions have been normalized.
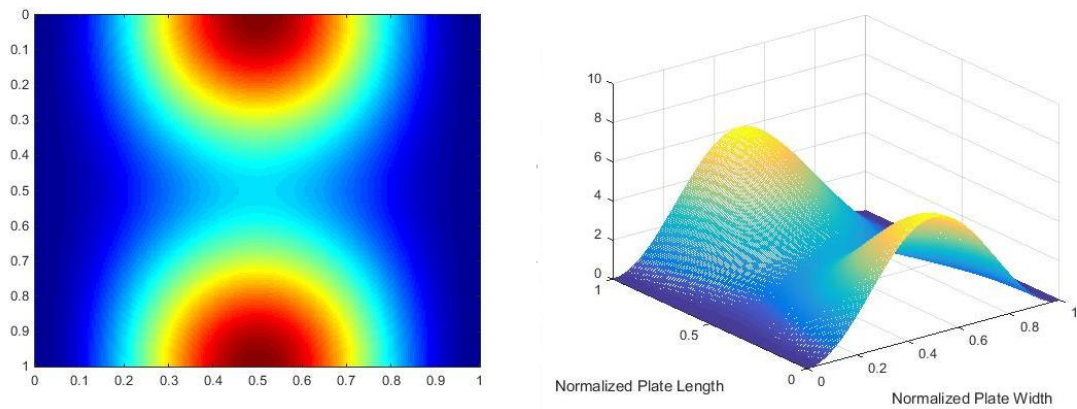
Figure 4.2: **Mode Shape Pressure Loading** - Normalized representation of pressure loading that deforms the plate in a manner similar to the shape of the fundamental frequency of the plate vibrating in air.
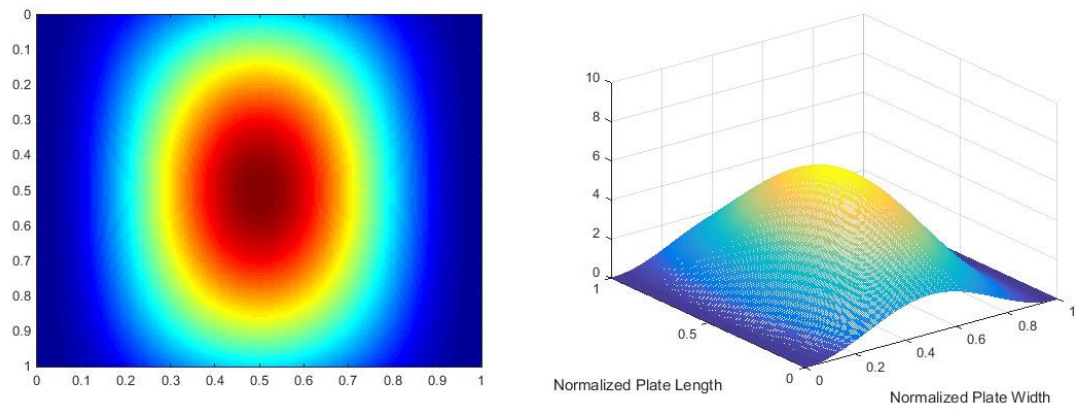
Figure 4.3: **Submerged Plate Pressure Loading** - Normalized representation of the pressure loading used to pluck submerged plates.

5 –Results

5.1   Air Results

Initially the Eigen frequency results, listed in Appendix A.2.1, were compared against one another, and the general trends observed to ensure the numeric models acted as anticipated. The numeric results were further compared against analytic results, listed in Table A.4 noting good comparisons. Then, data from the two clamped plate holders was compared against each of the three 'clamped plate' numeric boundary conditions, to establish which modeling condition yielded the best fit to experimental data. The Sinusoidal Slot data was compared against the numeric boundary conditions for both the flat and deformed plate assumptions.

5.1.1   Clamped Plates

General model validation was performed by comparing the effects of plate thickness and material on each of the three modeled clamped plate boundary conditions, shown in Figures 5.1 and 5.2. In Figure 5.1 the expected trend of thicker plates vibrating faster is seen, while in Figure 5.2 the difference between Inconel and Aluminum is minimal, while the the DU Plate has a significantly lower natural frequency.

Further comparisons between numeric and analytic results lends additional confidence to the Numeric models. A subset of plates, representing various lengths, thicknesses, and materials, are compared for all boundary conditions in Figure 5.3, with Figure 5.4 providing a more detailed comparison for the F-P boundary condition. It is noticeable that the numeric results are in good agreement with the analytic; excepting the DU Plate, which deviates for all three boundary conditions.
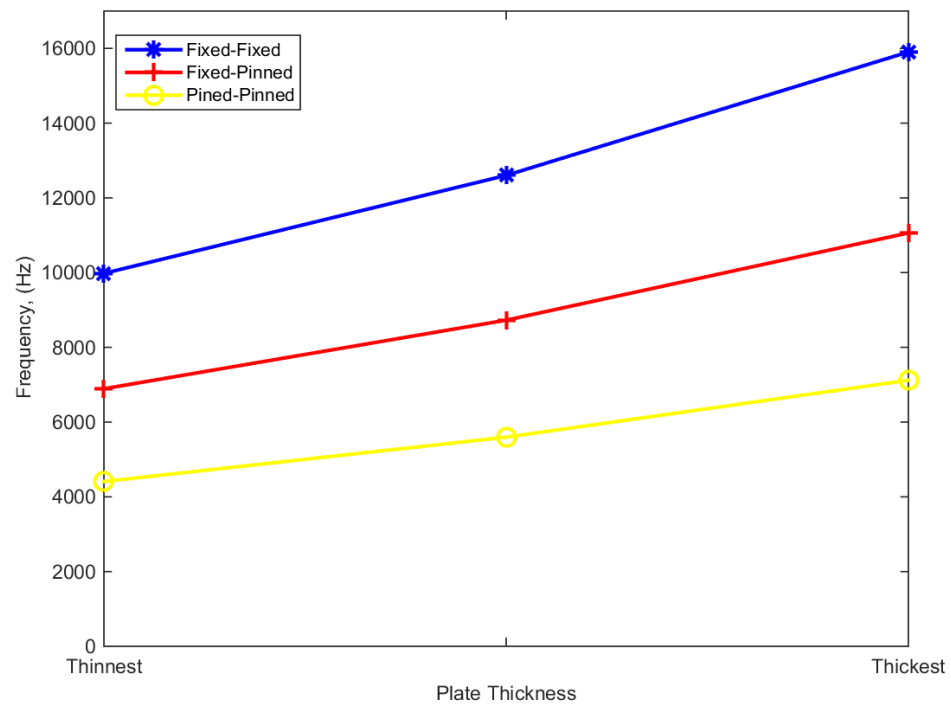
Figure 5.1: **Fundamental Frequency vs. Plate Thickness** - Numeric results for homogeneous Aluminum plates compared as a function of plate thickness
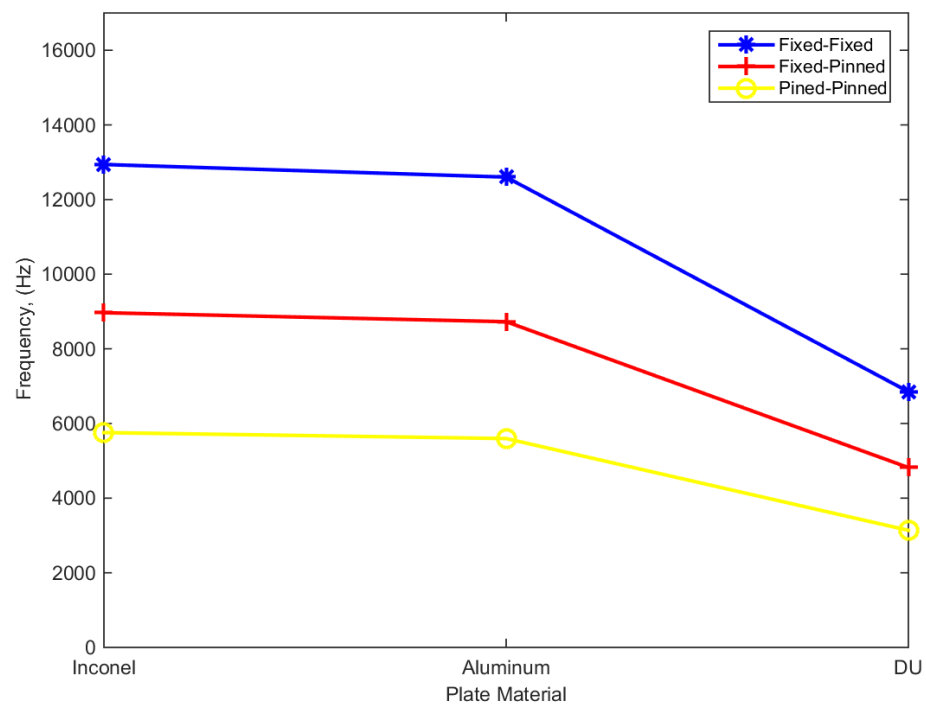
Figure 5.2: **Fundamental Frequency vs. Plate Material** - Numeric results compared as a function of plate material for homogeneous Aluminum and Inconel, as well as laminate DU plate
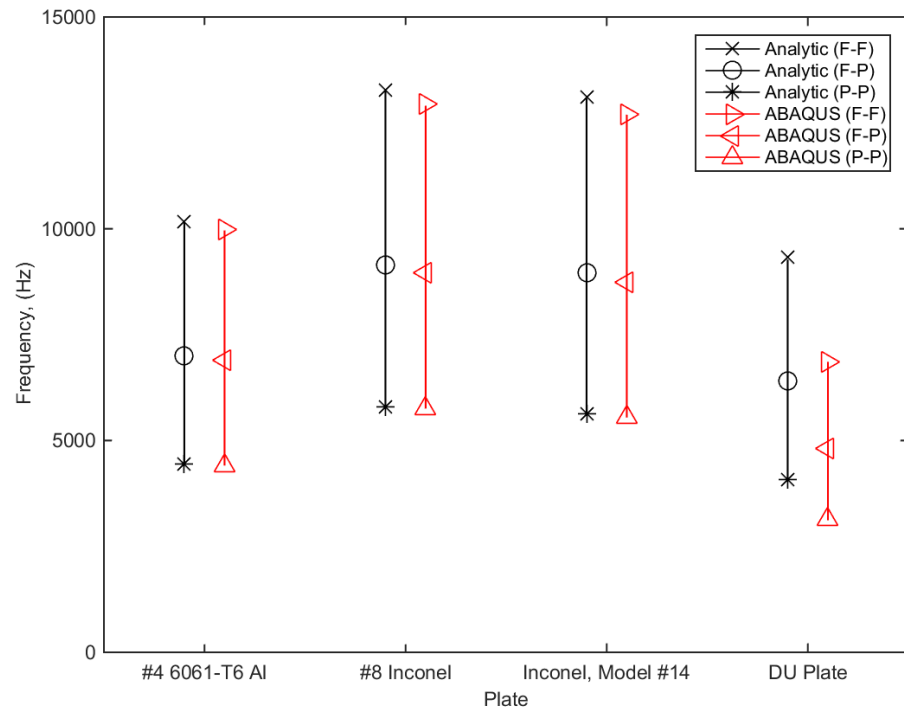
Figure 5.3: **Numeric and Analytic Comparison** - Comparison between Numeric and Analytic Results for all 3 boundary conditions, F-F, F-P and P-P
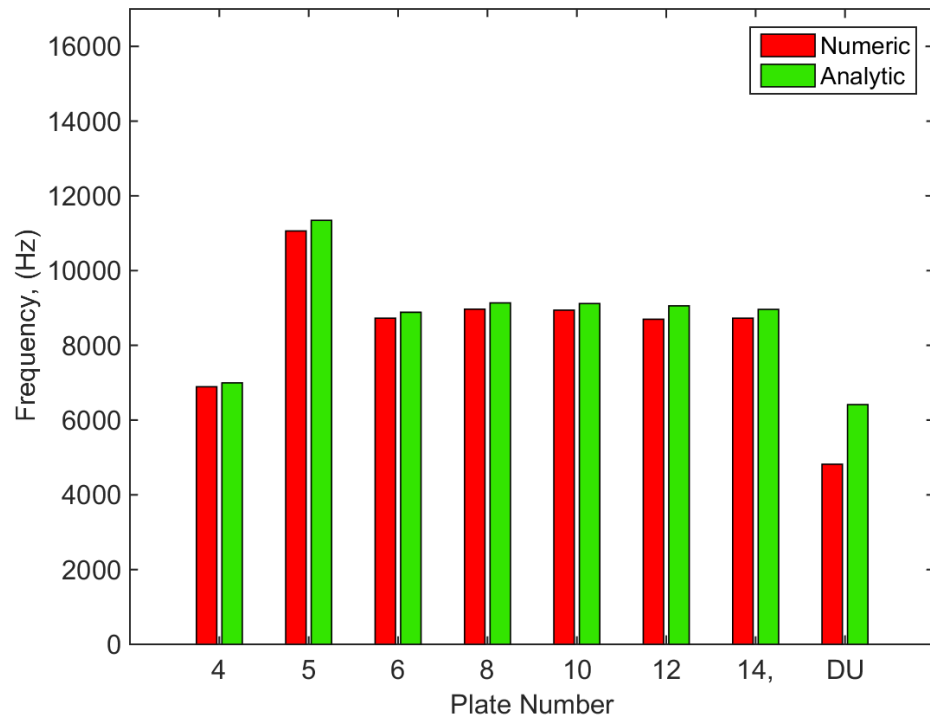
Figure 5.4: **Numeric vs. Analytic F-SS Comparison** - Comparison between the numeric and analytic results for a subset of plates for the F-P boundary condition

The clamped plate holders in the VFC should each yield slightly different data, due to the different boundary conditions, as shown in Figures 1.2 and 1.3. The different behaviors of the experimental plates under each of the two holders can be observed in Figure 5.5, and are listed in Appendix A.2.1.
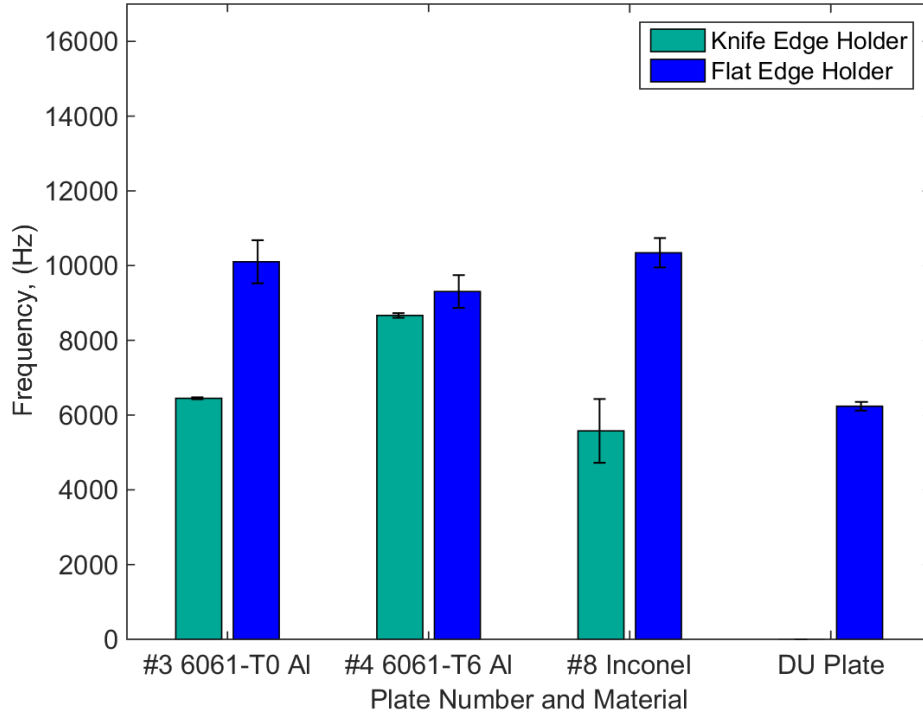
Figure 5.5: **Experimental Data Comparison** - Comparison of the experimental data from the flat and knife edge holders

These basic comparisons lend confidence to the Eigen solver results. Figure 5.6 shows that the numeric results do fall within the experimental data range; shown for both clamped plate holders and all three clamped boundary conditions. In further detail, Figures 5.7 to 5.9, show the set of experimental data compared against each of the three simulated boundary conditions. The experimental plate holders are not easily defined by a simple boundary condition; however in general, the F-P condition yields decent approximations for the Flat edge holder, while the P-P boundary condition

yields good approximations for the Knife edge, with the noticeable exception of the DU plate, for which the Flat edge data is most accurately modeled by the F-F condition.
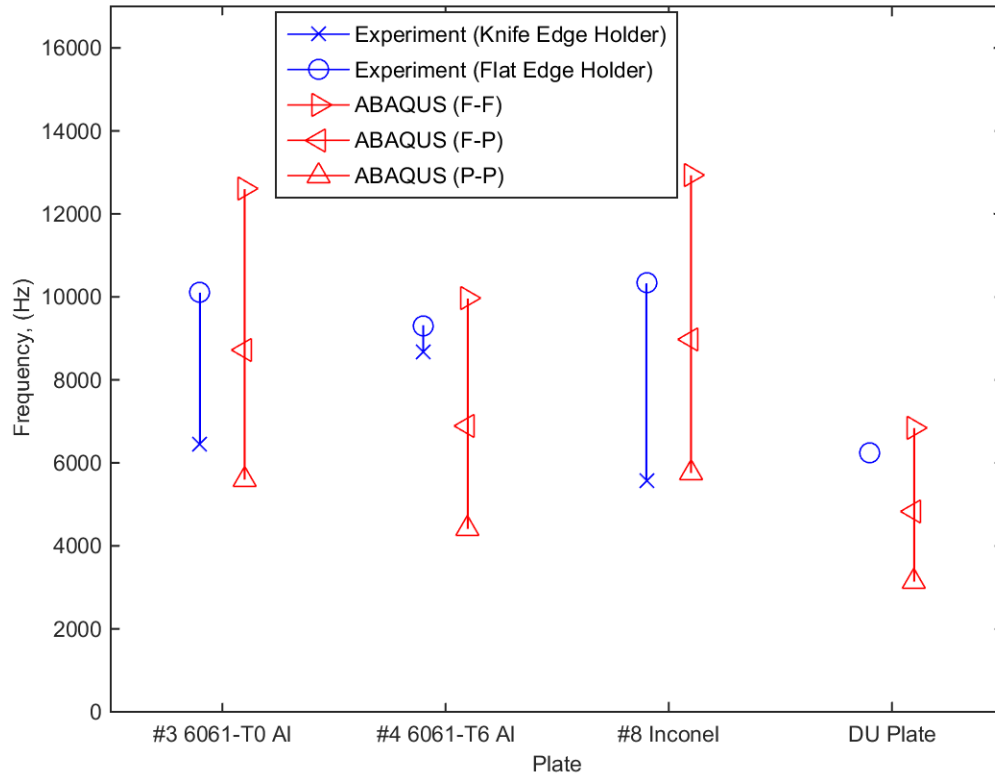
Figure 5.6: **Numeric vs. Experimental Comparison** - Comparison between the range of clamped plate experimental data and the range of clamped plate numeric results
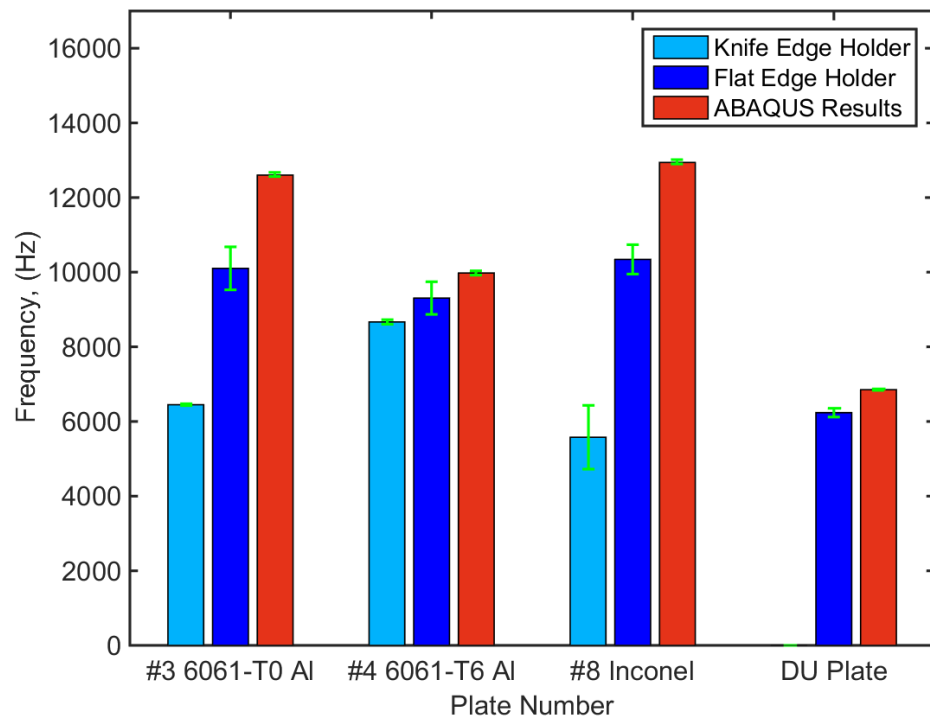
Figure 5.7: **Clamped Plate Experimental and Numeric F-F Comparison** - Comparison of the F-F numeric results against experimental data from the Flat and Knife edge plate holders
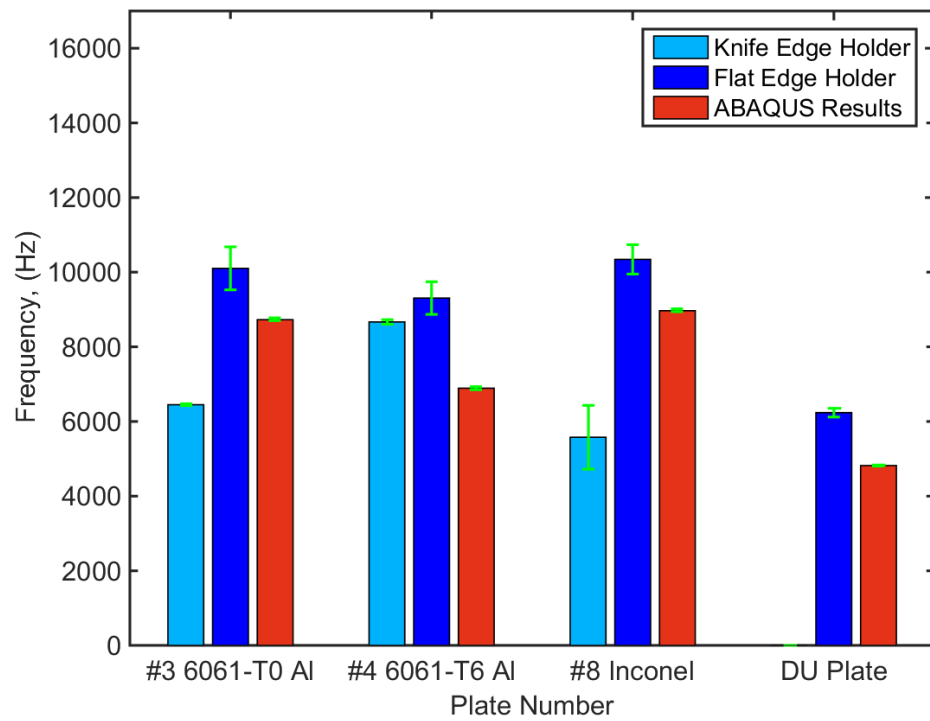
Figure 5.8: **Clamped Plate Experimental and Numeric F-P Comparison** - Comparison of the F-P numeric results against experimental data from the Flat and Knife edge plate holders
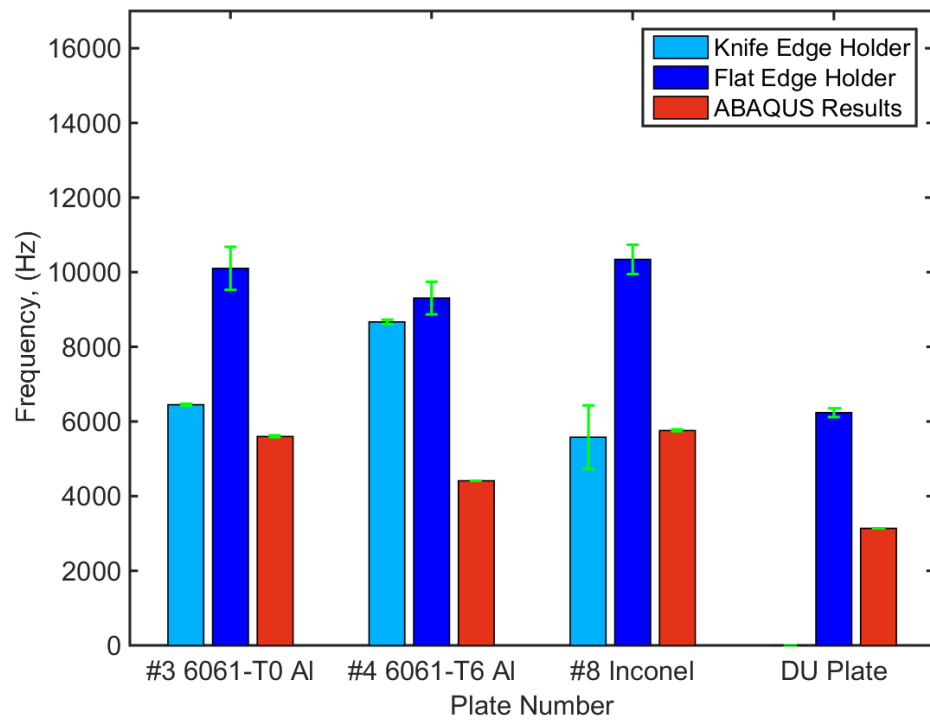
Figure 5.9: **Clamped Plate Experimental and Numeric P-P Comparison** - Comparison of the P-P numeric results against experimental data from the Flat and Knife edge plate holders

5.1.2   Sinusoidal Slot

For the Sinusoidal Slot, it becomes apparent that the deformed plate assumption is far more accurate than the flat plate assumption, especially for Out–of–Phase simulations. For the In–Phase comparison, shown in Figure 5.10, the experimental data has excessive amounts of error, likely a result of plate chatter within the slot, thus no conclusions about the modeling ability of either solution method can be drawn. Transitioning to Out–of–Phase models, the results of the flat plate assumption barely change, shown in Figure 5.11, but the deformed plate assumption compares quite well with experimental data.
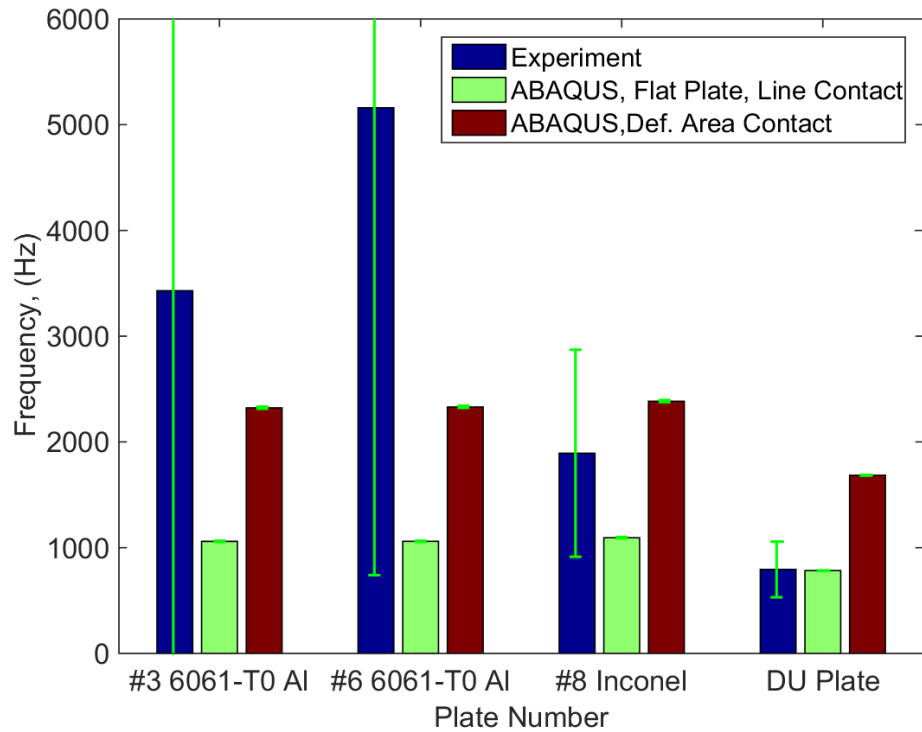
Figure 5.10: **In-Phase Boundary Condition Comparison** - Comparison between the Flat and the Deformed Plate Assumptions against the experimental data for the In-Phase Holder
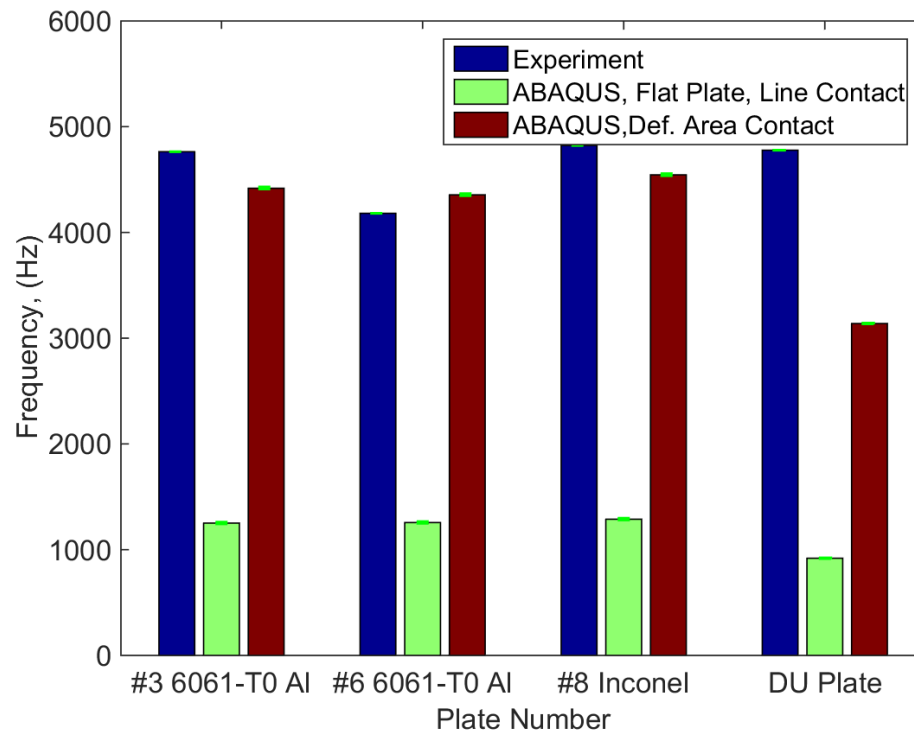
Figure 5.11: **Out-of-Phase Boundary Condition Comparison** - Comparison between the Flat and the Deformed Plate Assumptions against experimental data for the Out of-Phase Holder

5.1.3   Pressure Loading

Since the numeric results for the P-P boundary condition compare favorably against the experimental data and can be modeled with relative simplicity, submerged calculations initially focused on these plates. In order to solve the submerged frequency, a set of simulations were run for an isolated plate in a vacuum, comparing the dynamic implicit 'pluck' solution, against the Eigen frequency results.

The initial pressure loading, shown in Figure 4.1, simulated the guitar pick used to experimentally pluck the plates. The displacement data and the FFT, shown in Figure 5.12, are messy and yield a result of 8013 Hz, which does not compare well against Eigen frequency result of 7119 Hz. Changing the pressure loading to mimic the first mode shape, shown in Figure 4.2, gave a cleaner FFT, shown in Figure 5.13 and a frequency of 6961 Hz, which compares nicely against the Eigen result of 7119. Unfortunately, the addition of the water elements changed the fundamental mode shape, requiring a different pressure loading, shown in Figure 4.3, which produced a cleaner FFT, shown in Figure 5.14, for submerged simulations.
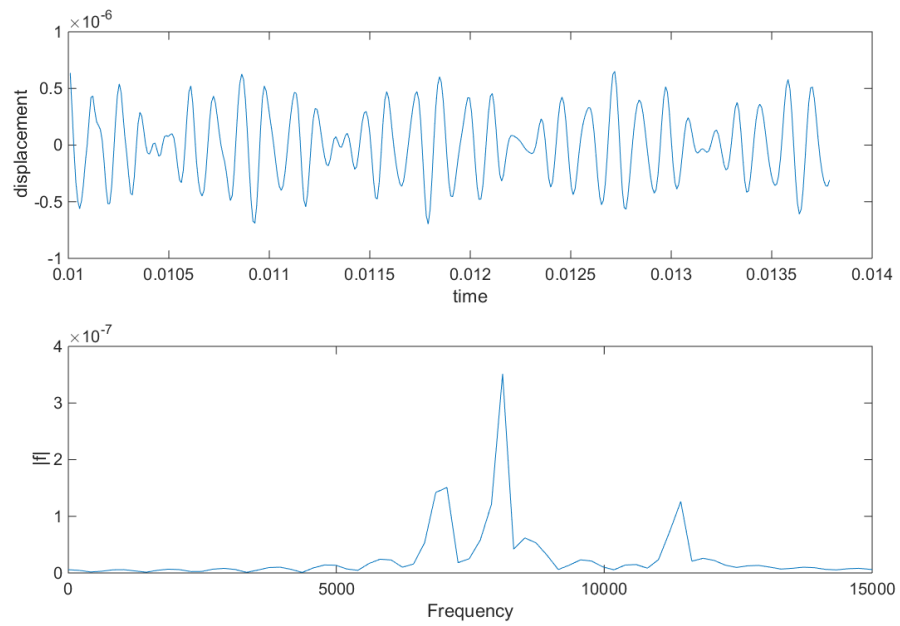
Figure 5.12: **Displacement and FFT results, Experiment Loading** - Displacement over time and the the Fourier Transform of that data for the guitar pick pressure loading of a simulated plate vibrating in a vacuum
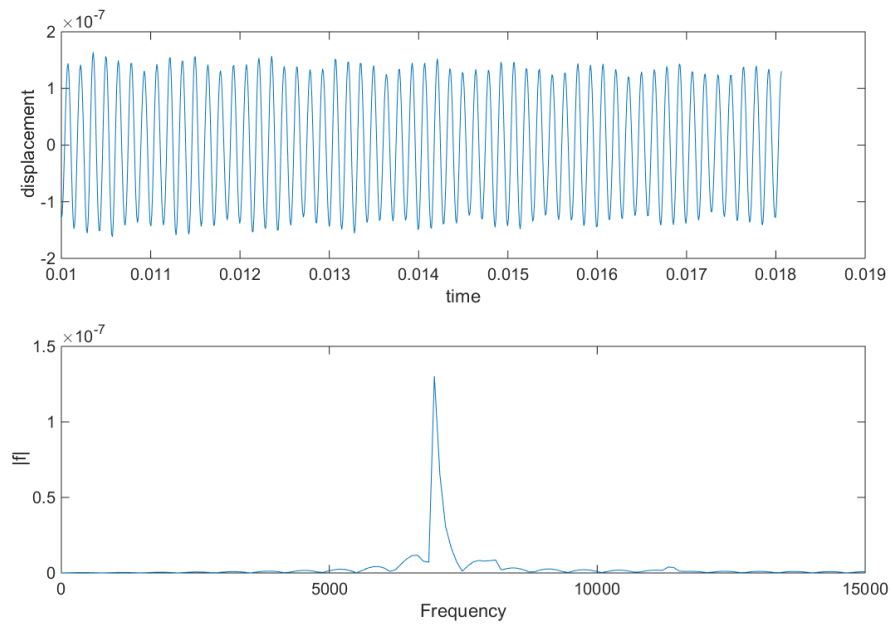
Figure 5.13: **Displacement and FFT results, Mode Shape Loading** - Displacement over time and the the Fourier Transform of that data, for the fundamental frequency of a simulated plate vibrating in a vacuum
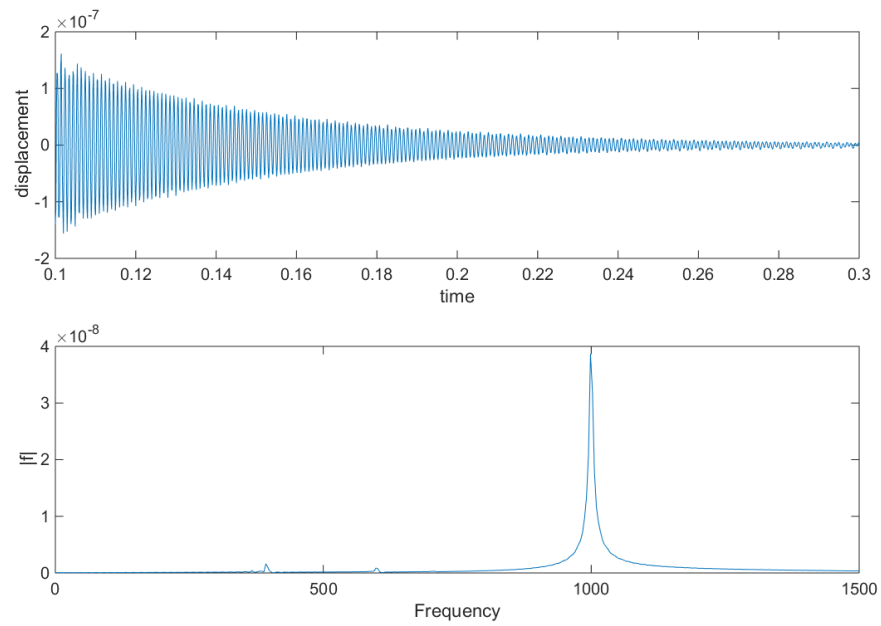
Figure 5.14: **Displacement and FFT results, Submerged Simulations** - Displacement over time and the the Fourier Transform of that data, for the fundamental frequency of a simulated submerged plate

5.1.4 Submerged Models

Before simulating numerous plates, the submerged results were compared against the isolated plate frequencies, to ensure that damping was occurring. As shown in Figure 5.15, the pseudo-fluid is significantly damping the plate frequencies, by over 2 orders of magnitude.
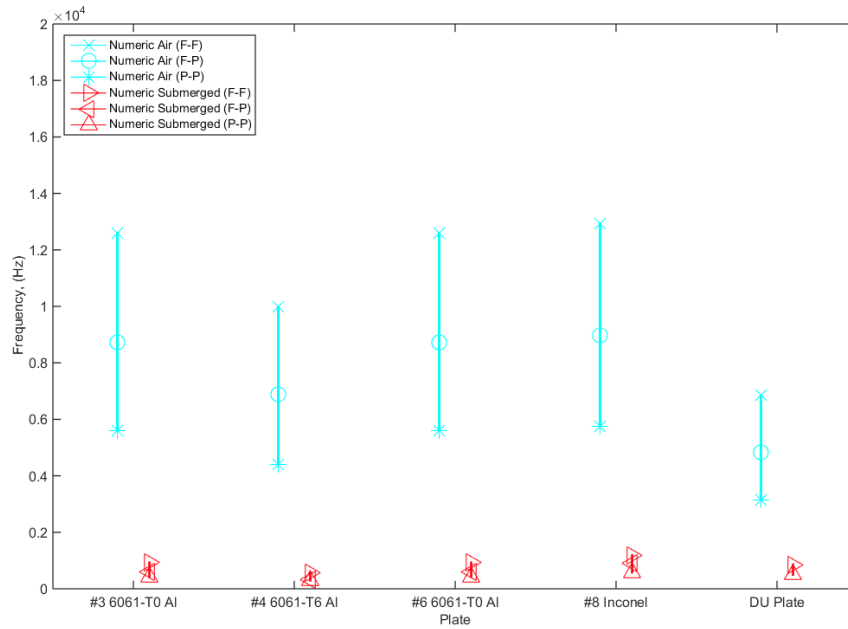
Figure 5.15: **Isolated Plate vs. Submerged Plate Frequency Comparison** - Numeric results for plates comparing the Eigen frequencies of the isolated plates against the dynamic solutions for the submerged plates, showing the large degree of damping occurring due to the pseudo-fluid.

The submerged modeling results are not easily defined by a certain characteristic. Shown in Figure 5.16, are the numeric results for the submerged plate simulations of the **A** and **B** channel gaps. The two channels line up closely with one another, as seen in detail in Figures 5.17 to 5.19, or in the tabulated data, listed in Appendices A.3.1 and A.3.2. In general, the **A** channel size has a lower frequency than the **B** channel.
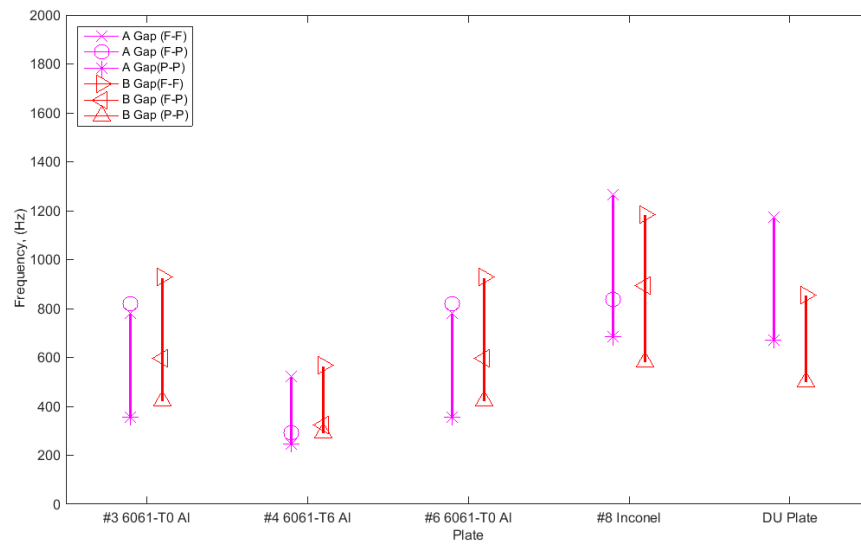
Figure 5.16: **Submerged Channel Gap Comparison** - Comparison of the numeric results for the **A** and **B** channel gaps for submerged plates.
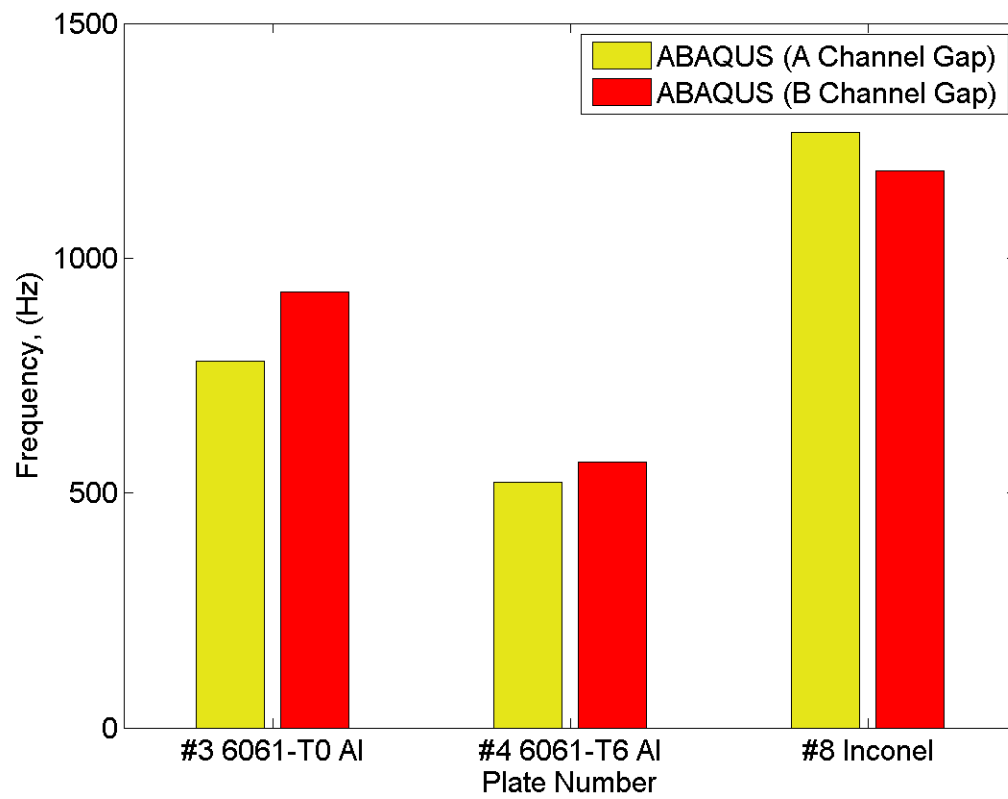
Figure 5.17: **Submerged F-F Channel Gap Comparison** - Comparison of the numeric results for the **A** and **B** channel gaps for submerged F-F plates.
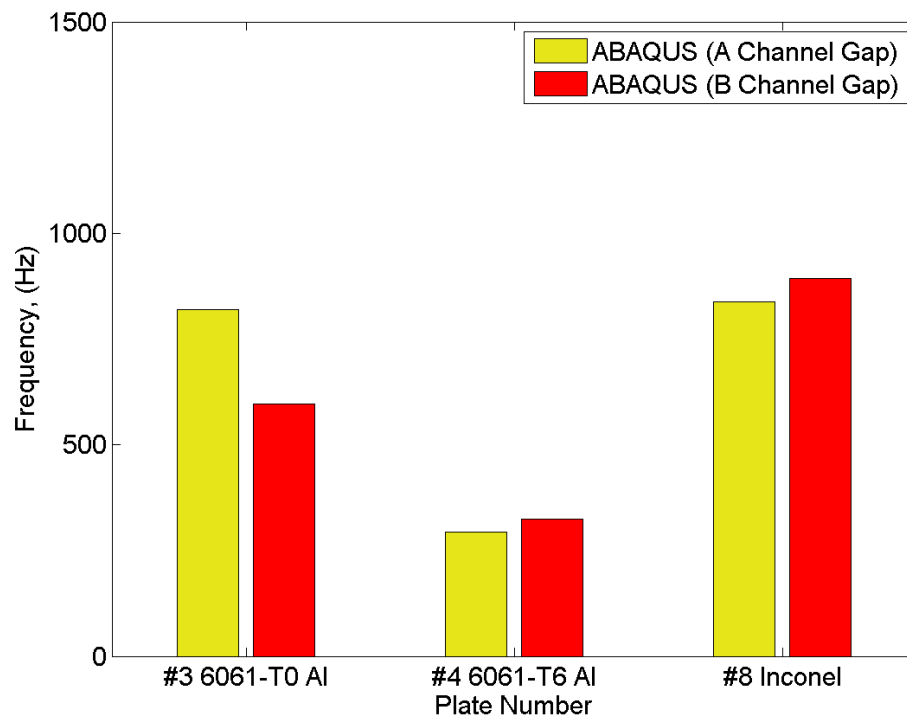
Figure 5.18: **Numeric vs. Analytic F-P Comparison** - Comparison between the numeric and analytic results for a subset of plates for the F-P boundary condition
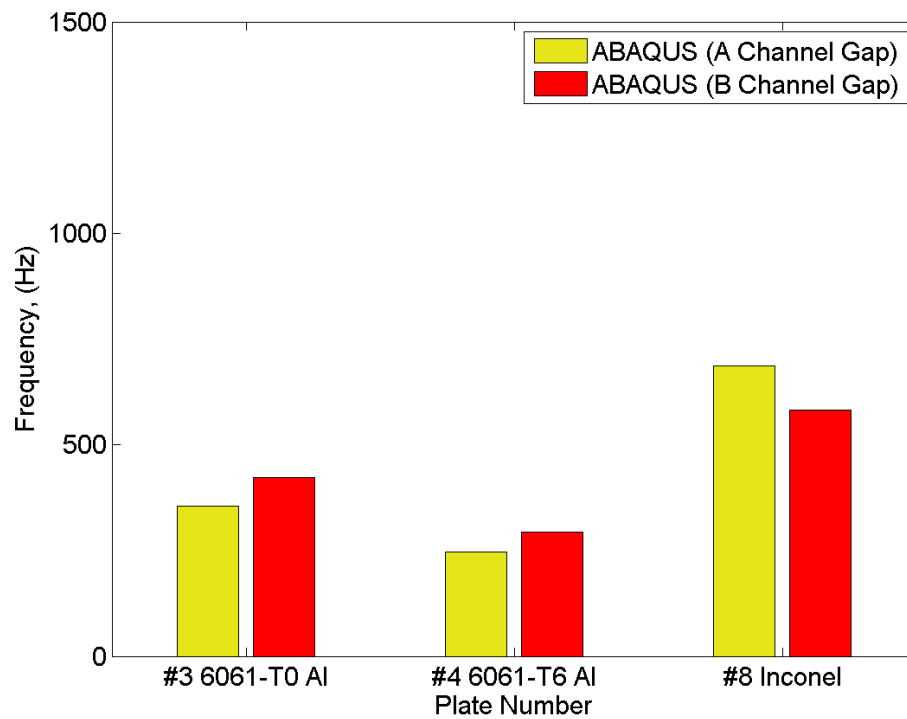
Figure 5.19: **Submerged P-P Channel Gap Comparison** - Comparison of the numeric results for the **A** and **B** channel gaps for submerged P-P plates.

Experimental data for the clamped plates is available for the B channel gap, which is compared against numeric results in Figure 5.20. In general the numeric results over-predict the submerged frequency, tabulated in Appendix A.3.2, with only the P-P condition giving results near experimental values, shown in Figure 5.21.
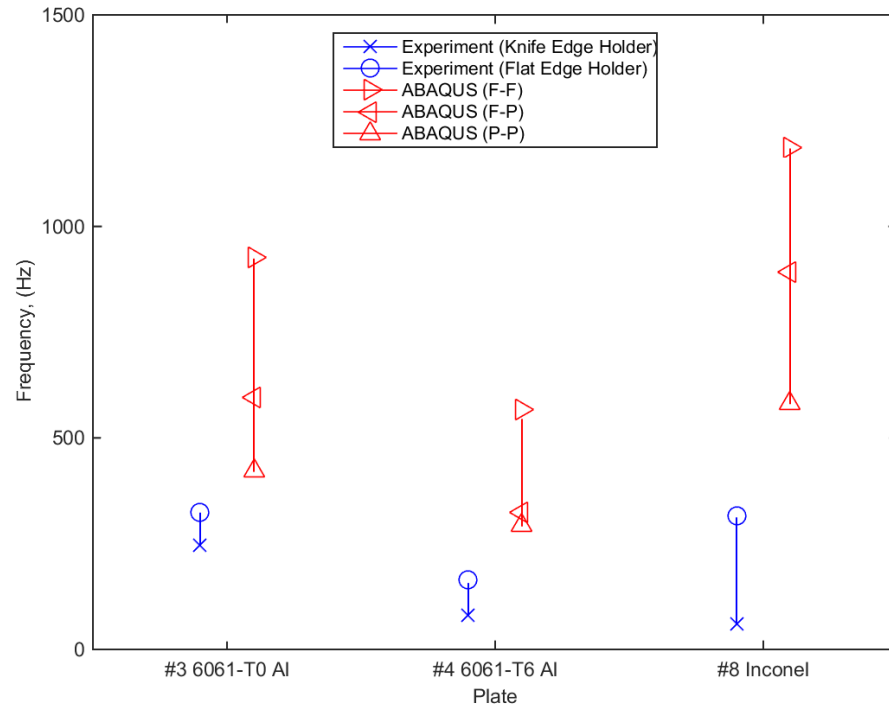
Figure 5.20: **Submerged Numeric vs. Experimental Comparison** - Comparison between the range of submerged experimental data and the range of submerged numeric results
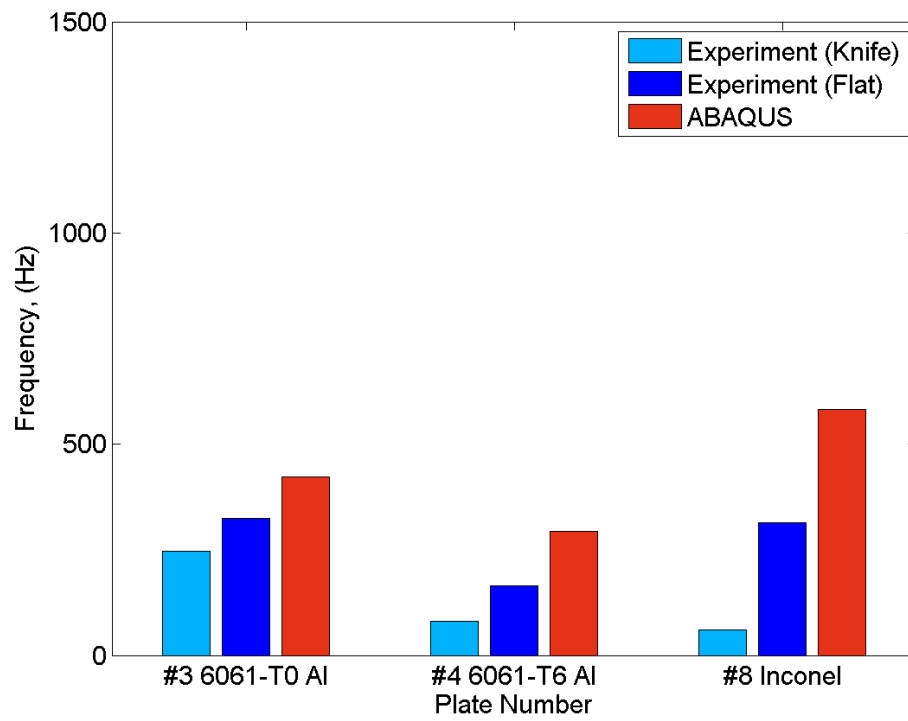
Figure 5.21: **Numeric vs. Experimental P-P Comparison** - Comparison between the numeric results and experimental data for a subset of plates, under the P-P boundary condition

6 –Conclusions

A numeric benchmark study was conducted to attempt to gain additional insight and understanding into submerged plate vibration, building off of a suite of experimental tests conducted at Oregon State University. The numeric results for fifteen plates under seven different boundary conditions, were compared against similar analytic results, and the experimental data from four plate holders. For the fundamental frequency of clamped plates vibrating in air, it was found that they are best modeled as an isolated plate with a width equal to the free vibration span of the holder, using either P-P line contacts for the Knife edge holder, or F-P contacts for the Flat edge holder. The Sinusoidal Slot is best modeled by deforming the plate through use of translating boundary conditions, applied over small area contacts to avoid massive stress concentrations. The Out–of–Phase simulations compare well against the numeric simulations, while the In–Phase experimental data has significant error, preventing the establishment of any conclusive trends. The flat plate assumption was not found to be accurate, especially for the Out–of–Phase holder. Modeling of the laminated plate presented numerous challenges, especially with consideration to the location of the foil within the plate. The assumption of a completely flat, perfectly centered foil was most likely the root cause of the significant departure of the DU results from the normal trends. In similar plates, it has been found that the foil sags during manufacturing, which may add significant stiffness to the plate.

Presently, numeric work suggests that the pseudo-fluid assumption has the potential to accurately predict submerged plate frequencies; however the small body of both numeric and experimental data does not present any obvious trends. Based on the in air studies conducted earlier, the dynamic implicit solver produces results very close to the Eigen frequency solver, which produces results near the experimental data for some cases, and follow easily identifiable trends. Building off of this knowledge, it is likely that further refinement of the modeling assumptions behind the pseudo-fluid

elements can yield accurate results that can be extended to a wide range of boundary conditions and plate materials, with accuracy trends mimicking those seen by isolated plates.

6.1   Suggestions for Future Work

Further work examining the laminate plate is necessary before numeric work can progress on it, particularly examining the discrepancy that exists between the numeric and analytic results, as shown in Figure 5.3, both of which assumed an ideal, flat foil, yet produce widely varying results; a discrepancy not observed in the comparisons between the homogeneous results. The ability to account for a deformed foil within the plate is necessary, since the foil sags within the cladding during manufacturing. The comparison of numeric results against experimental data showed that a stiffer boundary condition improved the accuracy of the results, and it is worth examining the applicability of various boundary conditions, or material properties, to see if it is possible to further increase accuracy and to derive trends that could be used for predictive purposes.

Further work on the pseudo-fluid method examining fluid properties, particularly the choice of Young's Modulus, presents another valuable line of inquiry, possibly yielding a more broadly applicable approach to increasing the simulation accuracy. Otherwise, further work expanding both the number of numeric results and body of experimental data, is likely to present general trends that would suggest additional methods for increasing accuracy. Using a different mesh, such as a quadratic element or switching to hybrid elements will help further increase the accuracy, at the cost of greatly increased solution times.

Bibliography

[1] T Howard, W Marcum, and W Jones. "Characterizing Virtual Mass Effects of a Submersed Body Using Pseudo-Fluid Elements". English. In: *The U.S. Role in a Global Nuclear Energy Enterprise*. Reno Nevada, June 2014, pp. 584–592.

[2] N. E. Woolstenhulme, S. D. Snow, and M. K. Meyer. *AFIP-6 Mk-II First Cycle*. Tech. rep. INL/EXT-12-25170. Idano National Laboratory, Mar. 2012.

[3] Paul Harmon et al. "On the Natural Frequency of Fueled Experimental Plates in Air and Water - Experimental Study". In: *2014 American Nuclear Societ Winter Meeting* 111 (2014), pp. 1654–1655.

[4] K. Bhaskar and T. K. Varadan. *Plates : Theories and Applications*. 1st ed. Hoboken: Wiley, 2014. ISBN: 9781118894804.

[5] Seon M. Han, Haym Benaroya, and Timothy Wei. "Dynamics of Transversely Vibrating Beams Using Four Engineering Theories". English. In: *Journal of Sound and Vibration* 225.5 (1999), pp. 935–988.

[6] Daniel J. Inman. "Distributed-Parameter Systems". English. In: *Engineering Vibration*. 1st ed. Prentice-Hall Inc., 1994, pp. 304–365. ISBN: 0139517731.

[7] Clarence W. de Silva. "Distributed-Parameter Systems". English. In: *Vibration Fundamentals and Practice*. 1st ed. CRC Press LLC, 1999, pp. 267–336. ISBN: 0849318084.

[8] Robert Blevins. *Formulas for Natural Frequency and Mode Shape*. English. 3rd ed. Florida: Krieger Publishing Company, 2001. ISBN: 1575241846.

[9] Y Kerboua et al. "Hybrid Method for Vibration Analysis of Rectangular Plates". In: *Nuclear Engineering and Design* 237 (2007), pp. 791–801.

[10] Shahed J. Hamedani, Mohammad R. Khedmati, and Saeed Azkat. "Vibration Analysis of Stiffened Plates using Finite Element Method". English. In: *Latin American journal of Solids and Structures* 9 (2012), pp. 1–20.

[11] Horace Lamb. "On the Vibration of an Elastic Plate in Contact with Water". In: *Proceedings of the Royal Society of London. Series A, Containing Papers of a Mathematical and Physical Character* 98.690 (Nov. 1920), pp. 205–216. URL: `hmmt://www.jstor.org/stable/93996`.

[12] MR Haddara and S. Cao. "A Study of the Dynamic Response of Submerged Rectangular Flat Plates". English. In: *Marine Structures* 9.10 (1996), pp. 913–933. ISSN: 0951-8339.

[13] V. Vu, M. Thomas, and L. Marcuiller. "Effect of Added mass on Submerged Vibrated Plates". English.

[14] N. C. Pal, P. K. Sinha, and S. K. Bhattacharyya. "Finite Element Dynamic Analysis of Submerged Laminated Composite Plates". In: *Journal of Reinforced Plastics and Composites* 20.07 (2001), pp. 547–564. DOI: `10.1177/073168401772678599`. URL: `http://jrp.sagepub.com/content/20/7/547`.

[15] P. Jensen and W. R. Marcum. "Predicting Critical Flow Velocity Leading to Laminate Plate Collapse-Flat Plates". English. In: *Nuclear Engineering and Design* 267 (2014), pp. 71–87. DOI: `10.1016/j.nucengdes.2013.11.071`.

[16] *Bulk Modulus and Fluid Elasticity*. URL: `http://www.engineeringtoolbox.com/bulk-modulus-elasticity-d_585.html` (visited on 01/20/2015).

[17] *Comparison Natural Frequency Calculations*. English. Tech. rep. Idaho National Laboratories, 2014, p. 3.

[18] Daniel T. DiPerna, William K. Blake, and Xingguang Z. DiPerna. "Computation of the homogeneous and forced solutions of a finite length, line-driven, submerged plate". In: *The Journal of the Acoustical Society of America* 120.6 (Dec. 2006), pp. 3664–3671. ISSN: 0001-4966. DOI: `10.1121/1.2357716`. URL: `http://scitation.aip.org.ezproxy.proxy.library.oregonstate.edu/content/asa/journal/jasa/120/6/10.1121/1.2357716` (visited on 02/16/2015).

[19]   *Global Threat Reduction Initiative — National Nuclear Security Administration.* URL: http://nnsa.energy.gov/aboutus/ourprograms/dnn/gtri (visited on 08/05/2014).

[20]   *GTRI Convert program National Nuclear Security Administration.* URL: http://nnsa.energy.gov/aboutus/ourprograms/dnn/gtri/convert (visited on 08/05/2014).

[21]   Maurice Petyt. *Introduction to Finite Element Vibration Analysis.* English. 1st ed. Cambridge University Press, 1990. ISBN: 0521266076.

[22]   R. J. Fritz. "The Effect of Liquids on the Dynamic Motions of Immersed Solids". In: *Journal of Engineering for Industry* 94.1 (1972), pp. 167–176. ISSN: 0022-0817.

A –Tabulated Values used in Report

This appendix contains all numeric values used in the creation of tables and figures shown throughout the paper as well as additional numeric data not presented due to lack of experimental comparison.

A.1 Tabulated Values used in computations

Table A.1: Given λ^2 values

| Edge Ratio | F-F | | F-P | | P-P | |
	Mode 1	Mode 2	Mode 1	Mode 2	Mode 1	Mode 2
0.4	22.35	23.09	15.38	16.37	9.76	11.04
2/3	22.31	24.31	15.34	17.95	9.7	12.98
1	22.27	26.53	15.29	20.67	9.63	16.14
1.5	22.21	30.9	15.22	25.71	9.56	21.62
2.5	22.13	41.69	15.13	37.29	9.48	33.62

Table A.2: Extrapolated λ^2 values for VFC Plates

Plate	Edge Ratio	F-F		F-P		P-P	
		Mode 1	Mode 2	Mode 1	Mode 2	Mode 1	Mode 2
1	0.2483	22.38	22.62	15.4	15.71	9.78	10.17
2	0.2504	22.38	22.62	15.4	15.72	9.78	10.18
3	0.25	22.38	22.62	15.4	15.71	9.78	10.18
4	0.25	22.38	22.62	15.4	15.71	9.78	10.18
5	0.2509	22.38	22.62	15.4	15.72	9.78	10.18
6	0.2518	22.37	22.63	15.4	15.72	9.78	10.19
7	0.2508	22.38	22.62	15.4	15.72	9.78	10.18
8	0.2502	22.38	22.62	15.4	15.71	9.78	10.18
9	0.2501	22.38	22.62	15.4	15.71	9.78	10.18
10	0.5	22.33	23.49	15.37	16.9	9.74	11.71
11	0.7496	22.3	24.95	15.33	18.75	9.68	13.91
12	1.1202	22.25	27.55	15.27	21.87	9.61	17.45
13	1.6899	22.19	32.74	15.2	27.52	9.53	23.57
14	2.8486	22.11	46.09	15.11	41.8	9.48	38.13
DU	0.25	22.38	22.62	15.4	15.71	9.78	10.18

Table A.3: Final Air Vibration Mesh Element Sizes

Plate	Length (m)	Width (m)	Thickness (m)
1-9	1.5200 E-04	1.5200 E-04	7.6200 E-05
10-14	1.2446 E-4	1.2446 E-4	0.6223 E-4
DU	1.2446 E-4	1.2446 E-4	0.6223 E-4
Thin 'Water' channel	2.8956E-4	2.8956E-4	2.8956E-4
Thick 'Water' channel	3.7846E-4	3.7846E-4	3.7846E-4

A.2 Results for Air Vibration

A.2.1 Clamped Plates

Table A.4: Analytic Results for Fundamental Frequency of Clamped Plates in Air

	Frequency (Hz)		
Plate	F-F	F-P	P-P
1	16484	11343	7203
2	16484	11343	7203
3	12912	8885	5643
4	10165	6995	4442
5	16484	11343	7203
6	12906	8885	5643
7	12912	8885	5643
8	13276	9135	5802
9	13276	9135	5802
10	13246	9118	5778
11	13228	9094	5742
12	13199	9058	5701
13	13163	9017	5653
14	13116	8963	5624
DU	9319	6413	4073

Table A.5: Numeric Results for Fundamental Frequency of Clamped Plates in Air

Plate	F-F (Hz)	F-P (Hz)	P-P (Hz)
1	15904	11,061.00	7,119.80
2	15903	11,061.00	7,119.30
3	12601	8,726.70	5,596.40
4	9978.7	6,892.00	4,410.10
5	15903	11,061.00	7,119.40
6	12601	8,726.70	5,596.40
7	12601	8,726.70	5,596.40
8	12939	8,967.70	5,755.50
9	12939	8,967.70	5,755.50
10	12920	8,942.30	5726.8
11	12636	8,737.90	5,586.80
12	12599	8,698.90	5,547.90
13	12552	8,651.80	5,506.90
14	12697	8,727.40	5,543.50
DU Plate	6852.2	4819.1	3137.7

Table A.6: Experimental Data for Fundamental Frequency of Clamped Plates in Air

Plate	Knife Edge	Fixed
3	6450.0 ± 25	10103 ± 576
4	8666.3 ± 61.9	9307.2 ± 473.6
6	8698.5 ± 3311	6168.0 ± 1442
8	5577.0 ± 853	10343.0 ± 393
DU	—	6236 ± 116

A.2.2   Sinusoidal Results

Table A.7: Numeric Results for Fundamental Frequency of Sinusoidal Plates in Air

Plate	In Phase		Out of Phase	
	Line Contact	Area Contact	Line Contact	Area Contact
3	1059.60	2321.6	1250.90	4418.2
4	834.62	1867.4	999.60	3478.3
6	1059.70	2330.3	1256.2	4355.5
7	1059.70	2325.5	1256.20	4391.9
8	1093.60	2384.0	1288.0	4544.4
9	1092.90	2382.9	1287.2	4544.0
DU Plate	783.52	1684.8	919.04	3138.9

Table A.8: Experimental Data for Fundamental Frequency of Sinusoidal Plates in Air

Plate	In–Phase	Out–of–Phase
3	3430.0 ± 3870	4763.0 ± 235
6	5160.0 ± 4420	4180.6 ± 47.4
8	1893.0 ± 979	4822.1 ± 39.8
DU	794.0 ± 263	4777.9 ± 29.5

A.3   Results for Submerged Plate Vibration

A.3.1   "A" Size water gap

Table A.9: Numeric Results for Submerged Fundamental Frequency of Clamped Plates with "A" Water Gap

Plate	Frequency (Hz)		
	F-F	F-P	P-P
4	523.44	292.73	246.00
6	781.25	820.31	355.47
8	1266.89	837.05	686.23
DU Plate	1171.9	—	671.87

Table A.10: Experimental Data for Submerged Fundamental Frequency of Sinusoidal Plates with "A" Water Gap

Plate	In–Phase	Out–of–Phase
3	—	260 ± 400
6	2520 ± 1970	952 ± 214
8	129.80 ± 94.30	59.0 ± 29.5
DU Plate	608.0 ± 373.0	766.8 ± 29.5

A.3.2   "B" Size water gap

Table A.11: Numeric Results for Submerged Fundamental Frequency of Clamped Plates with "B" Water Gap

Plate	F-F (Hz)	F-P (Hz)	P-P (Hz)
4	566.41	324.22	292.79
6	927.73	595.70	421.87
8	1185.8	892.86	582.03
DU Plate	856.33	—	500.00

Since the clamped plate holders restrict width, Plates 3 and 6 have identical dimensions within the holders and the experimental results for Plate 3 are compared against the numeric results from plate 6, since early error analysis on the submerged plates was conducted upon plate 6.

Table A.12: Experimental Data for Submerged Fundamental Frequency of Clamped Plates with "B" Water Gap

Plate	Knife Edge	Fixed
3	246.2	324.7
4	80	164.0
8	60	315

The submerged clamped plate experimental data presented in Table **??** was not collected as part of the VFF work, it was instead collected after the conclusion of the paper, using the same methods and equipment, but was not subject to the rigorous data analysis required to determine the standard deviation of each data set.

Table A.13: Experimental Data for Submerged Fundamental Frequency of Sinusoidal Plates with "B" Water Gap

Plate	In–Phase	Out–of–Phase
3	157.2 ± 41.9	519.0 ± 666
6	1370 ± 2010	1907.2 ± 42
8	231.0 ± 112	1091 ± 1224
DU Plate	808.0 ± 375	991 ± 885

B –Error Analysis Details

This appendix contains the error analysis calculations and results, performed according to Section 4.2. The first table presents the ABAQUS results and derived values from the ABAQUS results. The log values were plotted against one another in Excel 2013 and the results of the equation parameters of a best fit line are shown in the subsequent table. This table also includes the linear extrapolation predictions for each of the error analysis steps, which were used as a figure of merit for error checking the analysis.

B.1 Clamped Plate Error Analysis

Details of the grid analysis. The element edge length ratio used for all grid independence studies was 2:2:1 (l:w:t).

Table B.1: Plate 1 Error Analysis

elements across plate	Frequency	h	Δh	$log(\Delta h)$	$log(\Delta f)$	Δf
5	7032.7	0.2				
10	7093.2	0.1	0.1	-2.3026	4.102643	60.5
20	7117.3	0.05	0.05	-2.9957	3.182212	24.1

Table B.1: Plate 1 True Frequency Calculations

m	1.3279
b	7.1603
Extrapolated Value 1	7093.2
Extrapolated Value 2	7117.3
True Frequency	7141.4

Table B.2: Plate 4 Error Analysis

elements across plate	Frequency	h	Δh	$log(\Delta h)$	$log(\Delta f)$	Δf
5	4327.1	0.2				
10	4403.9	0.1	0.1	-2.3026	4.341205	76.8
20	4419.9	0.05	0.05	-2.9957	2.772589	16

Table B.2: Plate 4 True Frequency Calculations

m	2.263
b	9.552
Extrapolated Value 1	4403.9
Extrapolated Value 2	4419.9
True Frequency	4435.9

Table B.3: Plate 10 Error Analysis

elements across plate	Frequency	h	Δh	$log(\Delta h)$	$log(\Delta f)$	Δf
5	5658.1	0.2				
10	5706.7	0.1	0.1	-2.3026	3.858622	47.4
20	5726.8	0.05	0.05	-2.9957	2.944439	19.0

Table B.3: Plate 10 True Frequency Calculations

m	1.2738
b	6.8166
Extrapolated Value 1	5706.7
Extrapolated Value 2	5726.8
True Frequency	5746.9

Table B.4: Plate 11 Error Analysis

elements across plate	Frequency	h	Δh	$log(\Delta h)$	$log(\Delta f)$	Δf
5	5520.4	0.2				
10	5567.8	0.1	0.1	-2.3026	3.858622	47.4
20	5587.3	0.05	0.05	-2.9957	2.9957	19.5

Table B.4: Plate 11 True Frequency Calculations

m	1.2814
b	6.8092
Extrapolated Value 1	5567.8
Extrapolated Value 2	5587.3
True Frequency	5606.8

Table B.5: Plate 12 Error Analysis

elements across plate	Frequency	h	Δh	$log(\Delta h)$	$log(\Delta f)$	Δf
5	5482.0	0.2				
10	5529.0	0.1	0.1	-2.3026	3.850148	47.0
20	5548.4	0.05	0.05	-2.9957	2.965273	19.4

Table B.5: Plate 12 True Frequency Calculations

m	1.2766
b	6.7896
Extrapolated Value 1	5529.0
Extrapolated Value 2	5548.4
True Frequency	5567.8

Table B.6: Plate 13 Error Analysis

elements across plate	Frequency	h	Δh	$log(\Delta h)$	$log(\Delta f)$	Δf
5	5441.1	0.2				
10	5487.7	0.1	0.1	-2.3026	3.841601	46.6
20	5506.9	0.05	0.05	-2.9957	2.95491	19.2

Table B.6: Plate 13 True Frequenc Calculations

m	1.2792
b	6.7871
Extrapolated Value 1	5487.7
Extrapolated Value 2	5506.9
True Frequency	5526.1

Table B.7: Plate 14 Error Analysis

elements across plate	Frequency	h	Δh	$log(\Delta h)$	$log(\Delta f)$	Δf
5	5472.7	0.2				
10	5519.9	0.1	0.1	-2.3026	3.854394	47.2
20	5539.3	0.05	0.05	-2.9957	2.9652735	19.4
40	5543.5	0.025	0.025	-3.6889	1.435085	4.2

Table B.7: Plate 14 True Frequency Calculations

m	1.7452
b	7.9796
Extrapolated Value 1	5525.2
Extrapolated Value 2	5535.6
Extrapolated Value 3	5544.0
True Frequency	5548.2

Table B.8: DU Plate Error Analysis

elements across plate	Frequency	h	Δh	$log(\Delta h)$	$log(\Delta f)$	Δf
5	3071.4	0.2				
10	3128.6	0.1	0.1	-2.3026	4.046554	57.2
20	3137.7	0.05	0.05	-2.9957	2.208274	9.1

Table B.8: DU Plate True Frequency Calculations

m	2.6521
b	10.153
Extrapolated Value 1	3128.6
Extrapolated Value 2	3137.7
True Frequency	3146.8

B.2   Sinusoidal In-Phase Error Analyses using the Flat Plate Assumption

Performed on Plates 4, 7, and the DU Plate. As in Tables B.9, B.9

Table B.9: Sinusoidal Plate 4 Error Analysis under Flat Plate Assumption

elements across plate	Frequency	h	Δh	$log(\Delta h)$	$log(\Delta f)$	Δf
5	821.38	0.2				
10	833.42	0.1	0.1	-2.3026	2.488234	12.0
20	836.34	0.05	0.05	-2.9957	1.071584	2.92

Table B.9: Sinusoidal Flat Plate 4, True Frequency Calculations

m	2.0438
b	7.1942
Extrapolated Value 1	833.4
Extrapolated Value 2	836.3
True Frequency	839.3

Table B.10: Sinusoidal Plate 7 Error Analysis under Flat Plate Assumption

elements across plate	Frequency	h	Δh	$log(\Delta h)$	$log(\Delta f)$	Δf
5	1041.3	0.2				
10	1056.7	0.1	0.1	-2.3026	2.734367	15.4
20	1060.3	0.05	0.05	-2.9957	1.280934	3.60

Table B.10: Sinusoidal Flat Plate 7, True Frequency Calculations

m	2.0969
b	7.5626
Extrapolated Value 1	1056.7
Extrapolated Value 2	1060.3
True Frequency	1063.9

Table B.11: Sinusoidal DU Plate Error Analysis under Flat Plate Assumption

elements across plate	Frequency	h	Δh	$log(\Delta h)$	$log(\Delta f)$	Δf
5	766.88	0.2				
10	781.46	0.1	0.1	-2.3026	2.679651	14.6
20	783.52	0.05	0.05	-2.9957	0.722706	2.06

Table B.11: Sinusoidal Flat Plate 7, True Frequency Calculations

m	2.8233
b	9.1805
Extrapolated Value 1	781.5
Extrapolated Value 2	783.5
True Frequency	785.6

B.3 Sinusoidal In-Phase Error Analyses using the the Deformed Plate Assumption

Performed on Plates 4, 7, and the DU Plate

Table B.12: Sinusoidal Plate 4 Error Analysis under Deformed Flat Plate Assumption

elements across plate	Frequency	h	Δh	$log(\Delta h)$	$log(\Delta f)$	Δf
5	1835.9	0.2				
10	1865.0	0.1	0.1	-2.3026	3.370738	29.1
20	1870.8	0.05	0.05	-2.9957	1.757858	5.80

Table B.12: Sinusoidal Deformed Plate 4, True Frequency Calculations

m	2.3269
b	8.7286
Extrapolated Value 1	1865.0
Extrapolated Value 2	1870.8
True Frequency	1876.6

Table B.13: Sinusoidal Plate 7 Error Analysis under Deformed Plate Assumption

elements across plate	Frequency	h	Δh	$log(\Delta h)$	$log(\Delta f)$	Δf
5	2277.0	0.2				
10	2319.8	0.1	0.1	-2.3026	3.7565	42.8
20	2326.7	0.05	0.05	-2.9957	1.9315	6.90

Table B.14: Sinusoidal Flat Plate 7, True Frequency Calculations

m	26329
b	9.8191
Extrapolated Value 1	2319.8
Extrapolated Value 2	2326.7
True Frequency	2333.6

Table B.15: Sinusoidal Plate 7 Error Analysis under Deformed Plate Assumption

elements across plate	Frequency	h	Δh	$log(\Delta h)$	$log(\Delta f)$	Δf
5	1650.8	0.2				
10	1681.1	0.1	0.1	-2.3026	3.41115	30.3
20	1684.8	0.05	0.05	-2.9957	1.3083	3.70

Table B.16: Sinusoidal Flat Plate 7, True Frequency Calculations

m	3.0337
b	10.397
Extrapolated Value 1	1681.1
Extrapolated Value 2	1684.8
True Frequency	1688.5

B.4   Tabulated Error Estimates for Clamped Plates

Estimated difference between numeric value and actual grid independent result for clamped plates vibrating in air.

Table B.17: Clamped Plate Error

Plate	F-F (Hz)	F-SS (Hz)	SS-SS (Hz)
1	48.0	33.4	21.5
2	48.0	33.4	21.5
3	38.1	26.4	16.9
4	58.1	40.1	25.7
5	48.0	33.4	21.5
6	38.1	26.4	16.9
7	38.1	26.4	16.9
8	39.1	27.1	17.4
9	39.1	27.1	17.4
10	45.2	31.3	20.0
11	44.0	30.4	19.4
12	43.8	30.3	19.3
13	43.6	30.0	19.1
14	10.7	7.3	4.70
DU Plate	19.8	13.9	9.1